AGU PUBLICATIONS

JGR

Journal of Geophysical Research: Oceans

RESEARCH ARTICLE

10.1002/2015JC010893

Field evidence of beach profile evolution toward equilibrium

B. C. Ludka[1], R. T. Guza[1], W. C. O'Reilly[1], and M. L. Yates[2,3]

[1]Scripps Institution of Oceanography, University of California, San Diego, La Jolla, California, USA, [2]Saint-Venant Hydraulics Laboratory (ENPC, EDF R&D, CEREMA), Université Paris-Est, Chatou, France, [3]Technical Department of Water, Sea and Rivers, CEREMA, Margny-les-Compiègne, France

Key Points:
- Sand levels were surveyed quarterly to 8 m depth on five beaches for 3–10 years
- Waves were estimated by initializing a regional model with offshore buoys
- Beach profile evolution is well described by an equilibrium model framework

Supporting Information:
- Supporting Information S1

Correspondence to:
B. C. Ludka,
bludka@ucsd.edu

Citation:
Ludka, B. C., R. T. Guza, W. C. O'Reilly, and M. L. Yates (2015), Field evidence of beach profile evolution toward equilibrium, *J. Geophys. Res. Oceans*, *120*, 7574–7597, doi:10.1002/2015JC010893.

Received 1 APR 2015
Accepted 26 OCT 2015
Accepted article online 30 OCT 2015
Published online 20 NOV 2015

Abstract An equilibrium framework is used to describe the evolution of the cross-shore profile of five beaches (medium grain size sand) in southern California. Elevations were observed quarterly on cross-shore transects extending from the back beach to 8 m depth, for 3–10 years. Transects spaced 100 m in the alongshore direction are alongshore averaged into nineteen 700–900 m long sections. Consistent with previous observations, changes about the time average profile in many sections are captured by the first mode empirical orthogonal function (EOF). The first EOF poorly describes sections with hard substrate (less than roughly 80% sandy bottom) and also fails near the head of a submarine canyon and adjacent to an inlet. At the 12 well-described sections, the time-varying amplitude of the first EOF, the beach state A, describes the well-known seasonal sand exchange between the shoreline and offshore (roughly between 4 and 7 m depth). We show that the beach state change rate dA/dt depends on the disequilibrium between the present state A and wave conditions, consistent with the equilibrium concepts of Wright and Short (1984) and Wright et al. (1985). Empirically determined, optimal model coefficients using the framework of Yates et al. (2009a, 2011) vary between sections, but a single set of globally optimized values performs almost as well. The model implements equilibrium concepts using ad hoc assumptions and empirical parameter values. The similarity with observed profile change at five southern California beaches supports the underlying model equilibrium hypotheses, but for unknown reasons the model fails at Duck, NC.

1. Introduction

Worldwide, almost 1 billion people live at elevations within 10 m of present sea level and this population is increasing dramatically [*McGranahan et al*., 2007]. Sandy beaches provide recreational space, drive tourist economies, and protect coastal infrastructure from flooding and erosion. Sandy beaches are dynamic; in southern California, the beach width typically changes by 20 m between summer and winter. Understanding beach profile response to both energetic waves and calms will be crucial as rising seas encroach on coastal infrastructure and climate change modifies storm frequency and intensity [*Stocker et al*., 2013].

The time-averaged flux of sediment through a vertical cross section, the relatively small difference between onshore and offshore fluxes, is difficult to measure or model accurately. Process-based models of cross-shore beach profile evolution estimate sand level changes from cross-shore gradients of the net fluxes [*Roelvink and Brøker*, 1993]. These models require extensive tuning because many processes involved are understood poorly. XBeach [*Roelvink et al*., 2009], a widely used process-based model [*Callaghan et al*., 2013], has limitations. *McCall et al*. [2010] applied a nonphysical erosion limiter to XBeach in order to reproduce barrier island evolution during a hurricane. *Pender and Karunarathna* [2013] used XBeach to model annual to decadal beach profile change, switching between the original storm erosion module when the arbitrarily predefined storm wave height threshold was exceeded and a newly created recovery module during smaller wave conditions. Unibest-TC, another process-based model, allowed for net shoreward sediment transport and reproduced on and offshore sandbar migration, growth, and decay [*Ruessink et al*., 2007; *Walstra et al*., 2012]. However, the shoreline location was held fixed. Energetics models use parameterizations of hydrodynamic forcing and sediment response different from XBeach and Unibest-TC and also successfully simulate cross-shore sandbar migration [*Thornton et al*., 1996; *Gallagher et al*., 1998; *Hoefel and Elgar*, 2003; *Kuriyama*, 2012; *Dubarbier et al*., 2015]. Process-based models are in continual development and will ultimately provide quantitative understanding of profile evolution by coupling detailed understanding of each underlying process. Equilibrium profile models do not estimate sediment fluxes and instead rely on

the hypothesis that for given wave conditions, profiles tend asymptotically toward a unique equilibrium shape. If the equilibrium framework is shown to produce realistic macroscopic behavior, then equilibrium ideas can be used to evaluate and inspire process-based models.

Pelnard-Considére [1956] and *Bakker* [1968] coupled conservation of mass with a profile's tendency to maintain particular shapes to predict the spatial and temporal evolution of coastal contours. *Bruun* [1954] recognized recurring $x^{2/3}$ beach profile shapes (x is the cross-shore distance from the shoreline) in hundreds of observed beach profiles, and models designed to reproduce similar geometric shapes, using mass conservation fundamentally, have been used to describe profile evolution [*Kriebel and Dean*, 1985; *Larson and Kraus*, 1989; *Dean*, 1991; *Kriebel and Dean*, 1993]. *Holman et al*. [2014] superimposed sandbars on another profile shape. *Davidson and Turner* [2009] constructed a profile evolution model using a different spatial shape and a constant wave threshold to determine the sense (erosion or accretion) of profile evolution. Similar to *Pender and Karunarathna* [2013], the threshold does not depend on the present profile state or antecedent wave conditions. In the model developed below, the equilibrium shape, and the sense of profile evolution (shoreline erosion or accretion), is determined by the observations. Mass is not necessarily conserved in the observations or model.

Wright and Short [1984] identified descriptive two-dimensional equilibrium morphologies that depend on the value of the parameter, $\Omega = H_b/(w_s T)$, where H_b is the breaking wave height, w_s the sediment settling velocity, and T is wave period. *Wright et al*. [1985] noted that beach response to incident wave conditions is not instantaneous, but rather evolves toward the equilibrium state at a rate dependent on both the incident wave conditions and the present beach state (and hence the recent wave history). More recently, this concept demonstrates skill at predicting the observed alongshore-averaged bar crest position [*Plant et al*., 1999; *Pape et al*., 2010], shoreline location [*Miller and Dean*, 2004; *Yates et al*., 2009a, 2011; *Davidson et al*., 2013; *Castelle et al*., 2014; *Splinter et al*., 2014], and beach three dimensionality [*Plant et al*., 2006; *Stokes et al*., 2015] on a broad range of beaches.

Here the equilibrium hypothesis is further explored with up to 10 years of quarterly beach profiles at five southern California sites. Beach profile time series of this length, frequency, and spatial coverage, described in section 2, provide a unique opportunity to evaluate equilibrium profile models. In section 3, the state A of the evolving profile is characterized using empirical orthogonal function (EOF) analysis [*Winant et al*., 1975; *Aubrey*, 1979; *Aubrey et al*., 1980]. The relationship of A to incident waves is broadly consistent with the equilibrium framework of *Wright et al*. [1985] (section 4). *Aubrey et al*. [1980] and *Larson et al*. [2000] also related statistical modes to the wavefield, although they did not employ an equilibrium response. An equilibrium beach state model following *Yates et al*. [2009a, 2011] is developed and tested in section 5, and alternative model formulations are explored. In section 6, the model is extended from beach state A to the depth profile. As summarized in section 7, the similarity with observed profile change in southern California supports the underlying model equilibrium hypotheses, but for unknown reasons the model fails at Duck, NC.

2. Observations

2.1. Field Sites

Sand levels and waves are monitored at five beaches within an 80 km reach in San Diego County, southern California (Figure 1): Imperial Beach (IB), Torrey Pines (T), Cardiff (C), Solana (S), and Camp Pendleton (P). The sand is medium grained (median $D_{50} = 0.20 \pm 0.05$ mm) but with considerable alongshore and cross-shore variation (Table 1) [*Haas*, 2005; *Yates et al*., 2009b]. Hard substrate at some locations [*Moffatt and Nichol*, 2010] affects profile change. Imperial Beach has a few offshore cobble patches in the south, adjacent to the cobbly shoal of the Tijuana River mouth (1 km south of the southernmost considered transect). A 450 m, recreational pier is located at the IB central section, and there are two short 100–150 m jetties in the northern region. Torrey Pines has some cobble patches and reef in the north (Figure 2a), where Los Peasquitos lagoon mouth connects to the ocean (section T9, Figure 2a). Scripps submarine canyon is just offshore to the south (Figure 2a). Torrey Pines is the study location of *Shepard* [1950], *Inman* [1953], *Inman and Rusnak* [1956], *Winant et al*. [1975], *Aubrey* [1979], *Aubrey et al*. [1980], and others. Solana Beach has reef in the south and north (Figure 6a, discussed below), and the San Dieguito Lagoon mouth is a few 100 m south of the southernmost transect. Cardiff Beach has reef and cobble patches in the south (Figure 6a, discussed

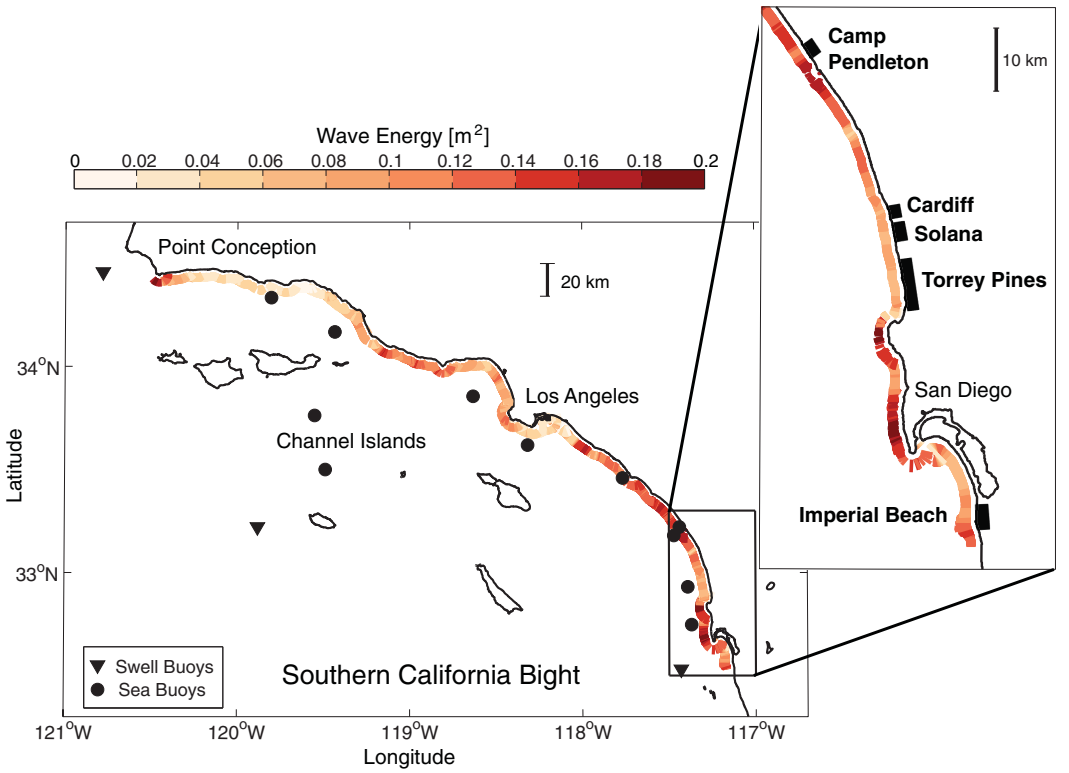

Figure 1. Plan view of southern California Bight. Wave buoys are used to initialize the swell wave propagation model (triangles) and to estimate local seas (circles). Inset shows zoom of region containing study beaches (black rectangles/bold labels). Colors show modeled wave energy every 100 m along the coast in 10 m water depth at 5:30 A.M. on 1 April 2012. Island shadowing causes significant gradients in wave energy along the coast.

below), and the San Elijo Lagoon mouth is a few 100 m north of the northernmost transect. Beach width and shoreface slope vary seasonally and alongshore. Typical values are in Table 1.

2.2. Waves

Waves are seasonal in southern California, with winter storms and summer calms. The offshore Channel Islands create coastal wave shadows [*Pawka*, 1983], and wave refraction over submarine canyons and other features contributes to alongshore variability in wave characteristics. Island blocking and refraction over local coastal bathymetry are modeled numerically (Figure 1). Swell wave (0.04–0.1 Hz) predictions are initialized with buoys near and seaward of the island system (triangles, Figure 1). Sea wave (0.08–0.5 Hz) propagation models are driven with nearby nearshore buoys (circles, Figure 1). Hourly directional wave properties are estimated every 100 m alongshore at Monitoring and Prediction (MOP) locations, in 10 m depth, and alongshore averaged within each 700–900 m long section (T8 is shown in Figure 2d). The swell model [*O'Reilly and Guza*, 1998] compares favorably with nearshore buoys in the present study area [*Young et al.*, 2012].

2.3. Sand Levels

Sand levels were measured on cross-shore transects spaced 100 m (50 m at Camp Pendleton) apart in the alongshore, from the backbeach to ~8 m depth (Figure 2a), using GPS-equipped platforms [*Seymour et al.*, 2005]. Bias and root-mean-square errors (RMSE, defined in Appendix A) are each roughly 10–15 cm. Although labor-intensive relative to remote sensing techniques, the errors are smaller [*Wengrove et al.*, 2013]. Approximately quarterly surveys were acquired for 3–10 years with alongshore spans between 1.4 km (Cardiff) and 7.3 km (Torrey Pines, Table 2). Profiles were created by bin-averaging elevation data in 20 m alongshore by 1 m cross-shore bins centered on the predetermined cross-shore transect lines, applying a 2 m cross-shore moving average, and splining to a 1 m grid wherever breaks in data do not exceed 20 m. Southern California beach profiles vary seasonally (Figure 2c). In summer, an elevated subaerial berm forms, while in winter the

Table 1. Survey Site Characteristics

Survey Site	Beach Width[a] (m)	Beach Slope[b]	MSL D_{50} (mm)[c]
Imperial	30–60	0.02–0.03	0.25
Torrey Pines	20–100	0.02–0.03	0.23
Solana	10–50	0.03–0.04	
Cardiff	20–40	0.03–0.04	0.16
Camp Pendleton	60–80	0.03	0.20

[a]Beach width is the time-averaged distance from the back beach to the MSL contour.
[b]Beach slope is calculated as the time-averaged slope between −1 and +1 m elevations relative to MSL. The beach face is concave; beach slope steepens higher on the beach.
[c]D50 is median grain size diameter.

subaerial beach erodes and an offshore bar develops [*Shepard*, 1950; *Winant et al.*, 1975; *Aubrey*, 1979; *Aubrey et al.*, 1980; *Yates et al.*, 2009a, 2009b].

Subaerial sand levels were measured more frequently (approximately monthly) at low tide on alongshore transects, spaced approximately 10 m apart in the cross shore (Figure 2b). Subaerial cross-shore transects with 1 m resolution were created by interpolating observations within 20 m wide alongshore swaths around the predetermined cross-shore transect line, onto the transect line. These subaerial measurements were not used in the analysis below but are sometimes shown to aid visual interpretation of the results.

On each transect, time series of sand level are created at the cross-shore locations with mean depths from −9 to +2 m (relative to MSL) at 1 m intervals. Transects missing more than half of the elevation data at these locations were discarded. Then, cross-shore locations missing more than half of the remaining time series were thrown out. Lastly, survey dates missing more than half of the remaining grid points were not used. The surveys were divided into 700–900 m alongshore sections, and elevation time series at each depth alongshore averaged, and the mean removed. After this, no more than 3% of the profile data were missing at each beach section and these gaps were linearly interpolated first in space and then in time for the analysis below. Torrey Pines sections (T1–T9) are shown in Figure 2a, and Cardiff (C1–C2) and Solana Beach (S1–S3) in Figure 6a (discussed below). The shoreline elevation for section T8 (green in Figure 2d,

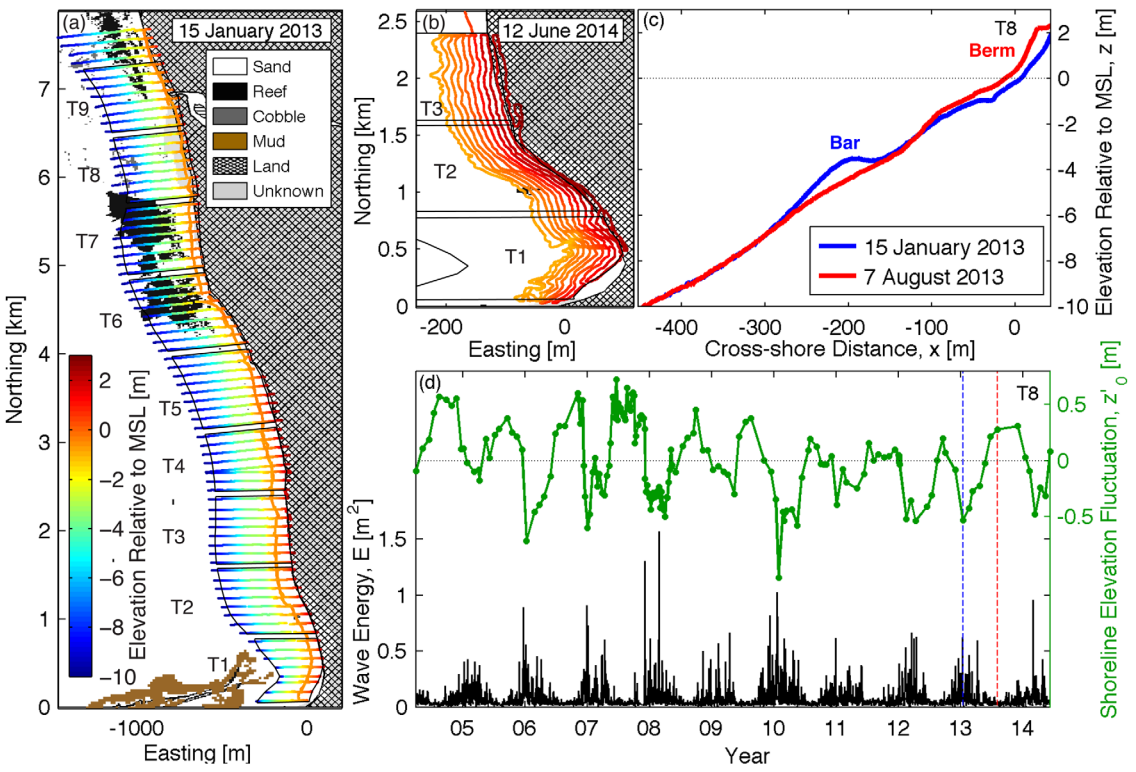

Figure 2. (a) Plan view of Torrey Pines Beach. Cross-shore survey transects (15 January 2013) are colored by depth (see color bar). Background colors/shading indicates substrate type (see legend) from multibeam and side scan sonar [*Moffatt and Nichol*, 2010]. Sections T1–T9 are indicated. (b) Plan view of T1–T3 sections showing colored-by-elevation subaerial (all terrain vehicle) survey tracks (12 June 2014). (c) Vertical elevation versus cross-shore distance for summer bermed (red) and winter barred (blue) profiles on a typical T8 transect. The shoreline $x = 0$ is the cross-shore location where the time-average sand elevation equals MSL. (d) Offshore (10 m depth) wave energy (black, left axis) and sand elevation at $x = 0$ (green, right axis) versus time. Results are averaged over the eight transects in section T8.

Table 2. Description of Survey Observations[a]

Survey Site	Alongshore Length (km)	Date Range	# Subaerial Surveys[b]	# Profile Surveys[c]	# Transects/Profile Survey
Imperial	2.1	Jan 2009 to Aug 2012	32	16	21
Torrey Pines	7.5	Apr 2004 to Jun 2014	138	36	74
Solana	2.3	May 2008 to Oct 2012	36	18	23
Cardiff	1.4	Jun 2007 to Oct 2010	44	16	14
Camp Pendleton	1.5	Feb 2007 to Oct 2010	31	14	30

[a]In total, more than 4000 km of survey tracks are analyzed.
[b]For the regions and time periods considered, and assuming six alongshore lines per subaerial survey (the typical number of lines on a narrow beach with a weak spring low tide; twice as many lines are driven on a wide beach with an extreme spring tide), over 2000 km of subaerial survey tracks have been driven.
[c]For the regions and time periods considered, and estimating 500 m as the typical length of a cross-shore profile transect, over 2000 km of profile survey track have been acquired.

including both subaerial and profile surveys) shows the expected summer accretion and winter erosion. Not surprisingly, vertical changes are reduced over (intermittently exposed) offshore reefs (e.g., Figure 3). Sand level changes are unusually large in the offshore portion of section T1 located near a submarine canyon (Figure 3).

3. Empirical Orthogonal Function Analysis

Empirical orthogonal function (EOF) analysis (Appendix B) [*Lorenz*, 1956] is used to decompose the profiles into the basic functions that most efficiently explain the data variance [*Davis*, 1976]. The first mode explains more variance than any other mode. Typical EOF mode 1 (hereafter EOF 1) temporal amplitude $A(t)$ (e.g., Torrey Pines section T8, Figure 4a) and spatial shape $W(x)$ functions (Figure 4b) correspond to a seasonal bar-berm rocking of sand between the shoreline (near mean sea level) and offshore (roughly 4–7 m depth) [*Winant et al.*, 1975; *Aubrey*, 1979; *Aubrey et al.*, 1980; *Yates et al.*, 2009a]. In summer, $A > 0$, and the profile is bermed. In winter, $A < 0$, and the profile is more strongly barred. Observed and reconstructed profiles using EOF 1 only are generally similar (Figures 4c and 4d), with the highest skill (defined in Appendix A) near the shoreline and offshore bar crest ($R^2 > 0.5$ near $x = 0$ and -200 m, blue curve in Figure 4e). Reconstruction

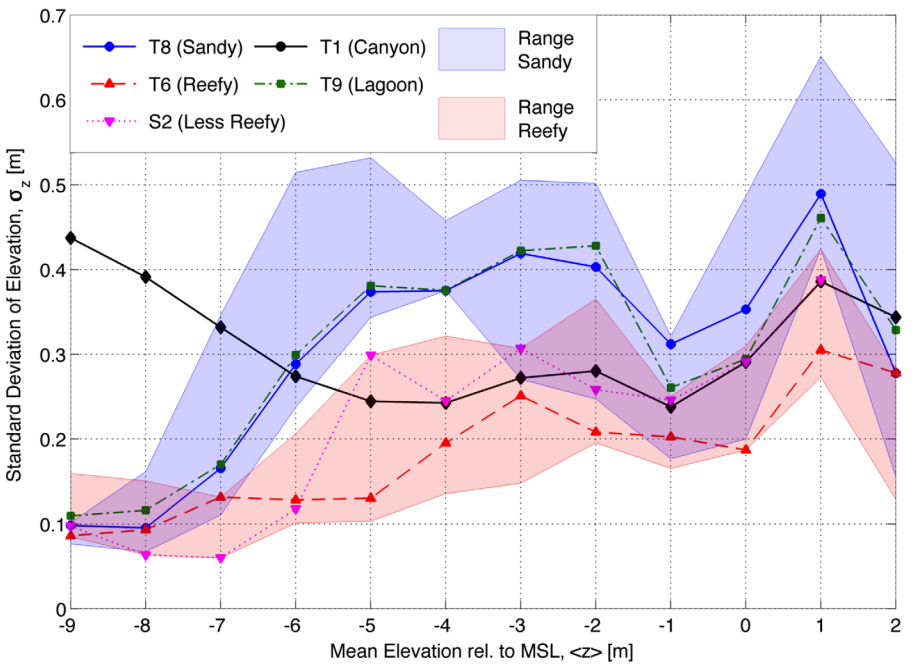

Figure 3. Standard deviation of elevation versus mean elevation for selected cross-shore transects (see legend). Standard deviation is lower at reefy (red swath) than sandy (blue swath) sections. Offshore (9 m mean depth) sand level fluctuations are anomalously large near a submarine canyon (T1, black).

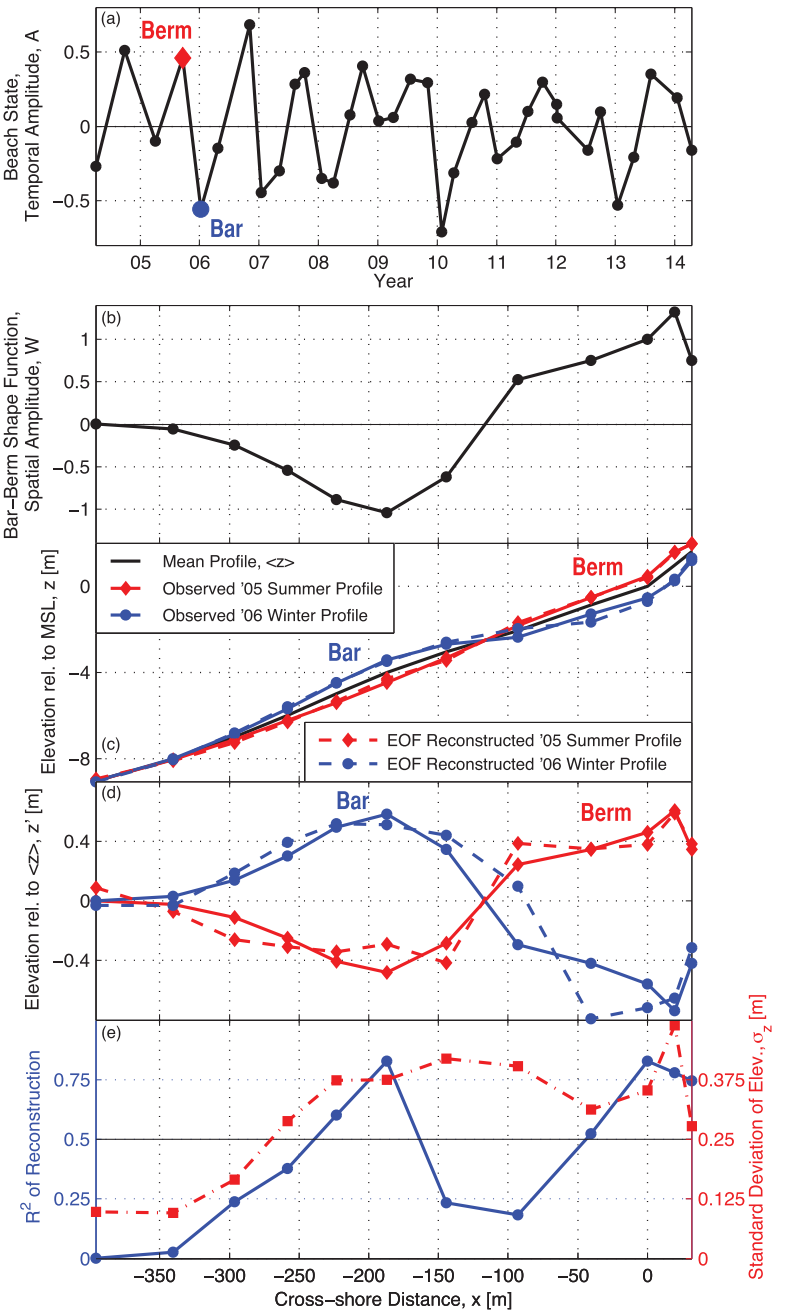

Figure 4. Torrey Pines, section T8. (a) Beach state (EOF 1 temporal amplitude *A*) versus time. (b) EOF 1 spatial weights *W* versus cross-shore distance *x*. (c) Elevation versus *x* for observed mean, summer, winter profiles (solid curves), and summer and winter EOF 1 reconstructions (dashed). (d) As in Figure 4c but with the mean profile removed to increase visibility. The observed and reconstructed profiles are similar, and EOF 1 describes 56% of the total (over all cross-shore locations) variance. (e) R^2 between observed and EOF-reconstructed sand level (solid blue curve) and standard deviation of observed elevation (red dash-dotted curve, right axis) versus *x*.

skill is low offshore ($x = -350$ m), but elevation fluctuations are small (standard deviation ~0.1 m, red dash-dotted line in Figure 4e). EOF 1 contains 56% of the total variance of all cross-shore locations at T8.

The empirical model for beach change developed below (sections 4 and 5) relies crucially on the existence of the spatially coherent fluctuations captured in EOF 1, similar to section T8 (Figure 4). Seasonal cross-shore rocking was at least weakly detectable at all sections (variation from purple to green in Figure 5a) except T1 just onshore of a submarine canyon. At T1, shaded gray in Figure 5a, the entire profile tends to rise and fall in tandem. Six additional sections were anomalous with either fewer than five substantially coherent cross-shore locations (purple diamonds in Figure 5c) and/or less than half the total variance

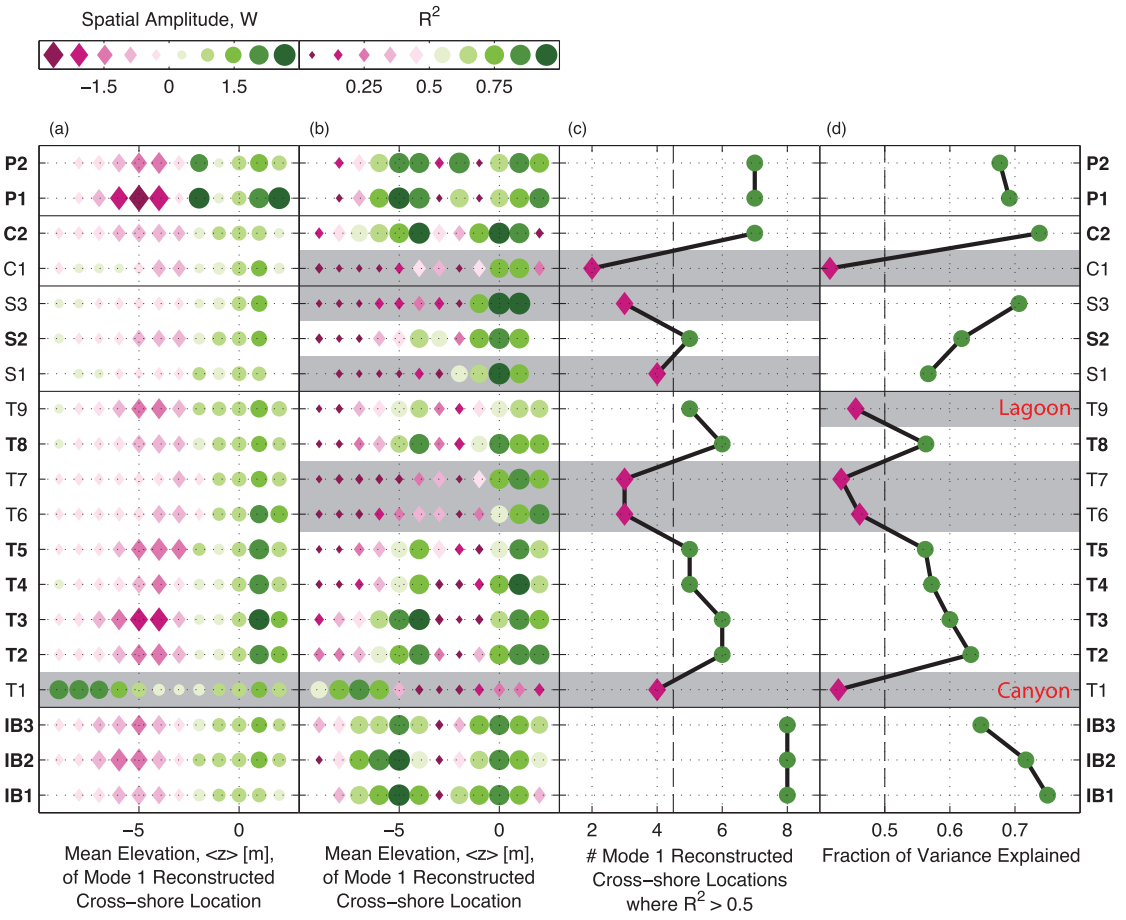

Figure 5. EOF performance at all sites. (a) EOF 1 spatial weights *W* versus mean elevation and section (*W* color bar at top). The anomalous *W* of T1 is shaded gray. (b) R^2 between observed and EOF-reconstructed sand level versus mean elevation and section (R^2 color bar at top). (c) Number of reconstructed cross-shore locations with $R^2 > 0.5$ at each section. In Figures 5b and 5c, sites with four or fewer cross-shore locations with $R^2 > 0.5$ are shaded gray. (d) Fraction of the total variance (all cross-shore locations) explained by EOF 1 at each section (ranging from 0.42 to 0.75, where shaded gray values are <0.5). Analysis is focused on the 12 sections well described by EOF 1 (bold on vertical axis and lacking gray shading).

explained (purple diamonds in Figure 5d). Anomalous sections are rocky (Figures 6a and 6b) [*Moffatt and Nichol*, 2010], and/or near a canyon or lagoon mouth (labeled in Figures 5 and 6). Twelve sandy sites (IB1, IB2, IB3, T2, T3, T4, T5, T8, S2, C2, P1, P2, unshaded sections in Figure 5, and bold axis labels in Figures 5 and 6b), away from reefs, a lagoon mouth, and a submarine canyon, were analyzed for equilibrium behavior.

4. Observational Evidence of Equilibrium Beach Profiles

The beach state change rate, dA/dt, and average wave energy, $\langle E \rangle$, between a pair of consecutive surveys are only weakly correlated (average $R^2 = 0.25$ at all 12 sections). Despite the low correlation, the results are consistent with equilibrium theory: the beach state change rate depends not only on the incident wave energy, but also on the present state of the profile. In Figure 7a, the beach state change rate between surveys, dA/dt, depends on both $\langle E \rangle$ and the state of the beach of the first of the two consecutive surveys, $A(t_0)$. For a given $\langle E \rangle$, the profile can change toward a more or less barred beach (color bar in Figure 7a), depending on $A(t_0)$. The observations are equilibrium like, but the details are distorted by wave averaging between surveys [*Yates et al.*, 2009a]. The equilibrium wave energy, E_{eq}, is the E for which a given initial beach state does not change (dashed black line drawn by eye in Figure 7a). If the beach is out of equilibrium with the incident waves, it moves toward the equilibrium shape. For example, with $\langle E \rangle = 0.068$ m^2 (black dotted horizontal line in Figure 7a), a beach with an initially eroded shoreline and developed offshore bar (left black dot, $A = -0.28$, Figure 7a, blue profile with circles in Figure 7b) will move toward the equilibrium profile (black line in Figure 7b) with offshore bar erosion and beach face accretion (blue arrows with circle base in Figure 7b). Conversely, with the same $\langle E \rangle$,

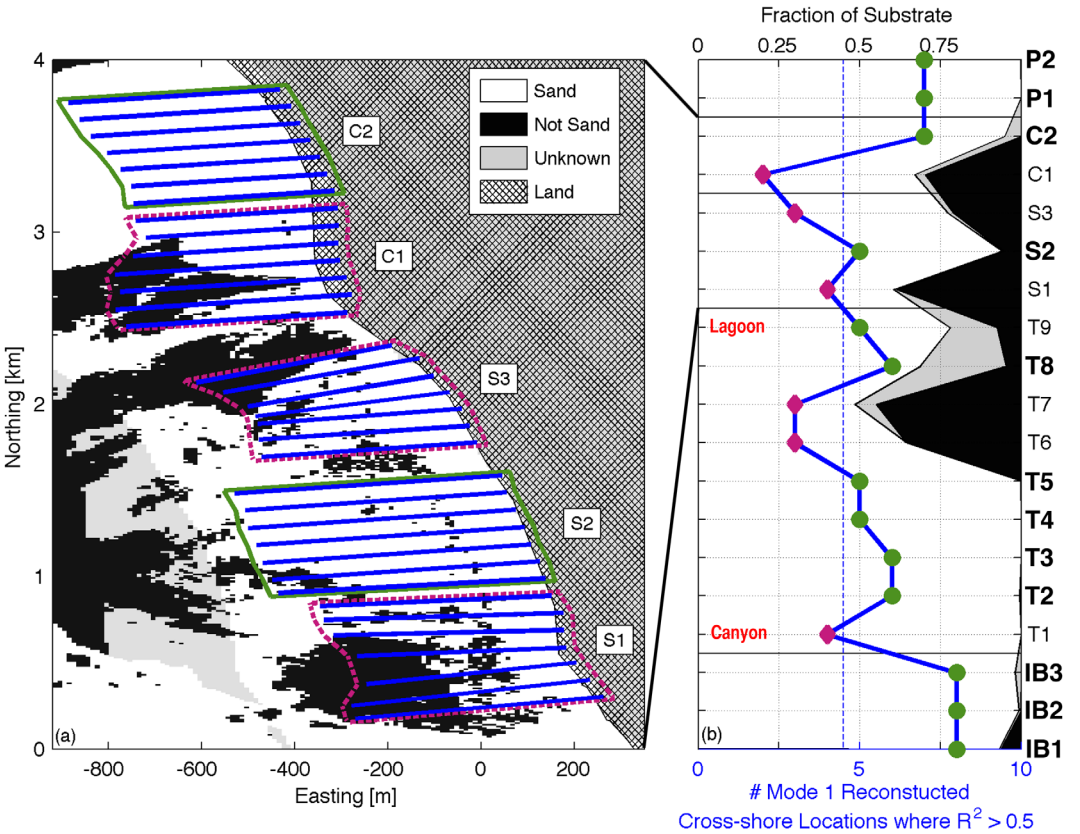

Figure 6. (a) Plan view of Cardiff (C1 and C2) and Solana (S1, S2, and S3) Beach sections and bottom type identified by multibeam and side scan sonar [*Moffatt and Nichol*, 2010]. Blue lines are survey cross-shore transects. Sections C2 and S2 (green solid line boxes) are well described by EOF 1, and C1, S3, and S1 (purple dotted boxes) are not. (b) For all sections, substrate type (top black axis) and number of cross-shore locations well described ($R^2 > 0.5$) by the EOF 1 reconstruction (bottom blue axis) versus alongshore section. Sand substrate is white, unknown is gray, and "not sand" is black as in the legend in Figure 6a. With the exception of slightly cobbly sections IB1 and T8, substrate classified as "not sand" is reef. Sections with relatively low % sand tend to have relatively few locations that are well described by EOF 1. For example, section C2 is almost all sand, and 7 (of 12) cross-shore locations are well reconstructed by EOF 1 (in Figure 6b, values greater than 5 are green circles). Section C1 is about 70% sand, and only two cross-shore locations are well reconstructed by EOF 1 (in Figure 6b, values less than 5 are purple diamonds). The sections well described by EOF 1 in general are labeled in bold on the right axis of Figure 6b. Well-described sections have more than half their total variance explained by EOF 1 (see Figure 5d), and EOF 1 reconstructs five or more cross-shore locations with $R^2 > 0.5$ (as in Figures 5c and 6b). T1 is onshore of a submarine canyon and T9 contains a lagoon mouth.

a beach with a well-developed berm and no offshore bar (right black dot, $A = +0.28$, Figure 7a, red profile with diamonds in Figure 7b) moves toward the same equilibrium profile (black line in Figure 7b), with onshore berm erosion and offshore bar accretion (red arrows with diamond base in Figure 7b). Although wave averaging between surveys blurs Figure 7, dA/dt appears to increase when $\langle E \rangle$ is farther from the equilibrium wave energy E_{eq} (as the deviation from the dashed black line in Figure 7a increases). Figure 7 is similar to *Yates et al.* [2009a] for location of the MSL contour, but extended to the profile state. The axes (flipped) of Figure 7 resemble the axes of *Wright and Short* [1984, Figure 12] and *Wright et al.* [1985, Figure 9], but instead of descriptive 2-D beach states, the beach state is simplified to cross-shore profiles and quantified using the EOF. The present observations span intermediate states (Iribarren number 0.3–0.7), and $A > 0$ is more reflective than $A < 0$, according to *Wright and Short* [1984] and *Wright et al.* [1985]. The undistorted equilibrium energy relationship (solid black line in Figure 7a) is now estimated from the model using hourly wave conditions that resolve individual storms.

5. Equilibrium Beach State Model

5.1. State Model Formulation

A 1-D equilibrium beach profile state model is developed that extends the shoreline model of *Yates et al.* [2009a, 2011], which was inspired by *Wright and Short* [1984], *Wright et al.* [1985], and *Miller and Dean* [2004].

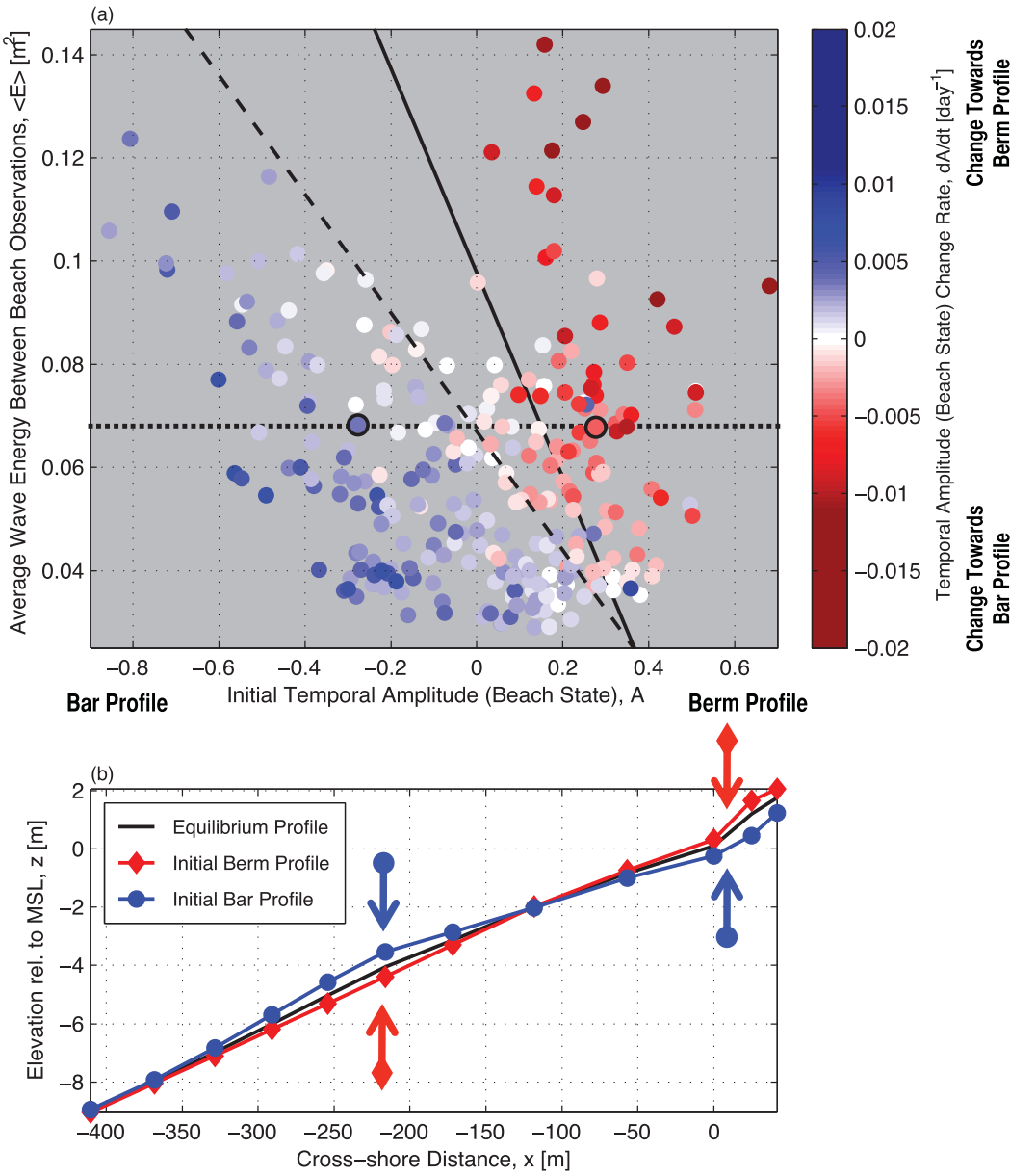

Figure 7. (a) Beach state change rate, *dA/dt* (see color scale), versus average wave energy between profile observations, $\langle E \rangle$, and initial beach state, *A*, for sections well described by EOF 1, where *A* is the temporal amplitude of EOF 1. The dashed black line (drawn by eye) separates change toward a barred profile (blue) from change toward a bermed profile (red). With $\langle E \rangle = 0.068$ m^2 (significant wave height $H_s = 1.04$ m, dotted black horizontal line), all profiles evolve toward $A_{eq} = -0.01$, the equilibrium state given by the intersection of the dotted and dashed black lines. The solid black line is the more accurate equilibrium relationship, calculated by optimizing model parameters (i.e., dashed vertical lines in Figure 10) in equations (1)–(3) using hourly waves. (b) Example initial and equilibrium profiles for the scenarios circled in black in Figure 7a. Arrows show the direction of beach change toward the equilibrium profile. The rate and direction of profile change depends not only on the incident wave energy, but also on the present beach state.

The instantaneous beach state change rate *dA/dt* is assumed proportional to the instantaneous energy *E* and energy disequilibrium ΔE

$$\frac{dA}{dt} = C^{\pm} E^{1/2} \Delta E, \tag{1}$$

where $C^{\pm}$ are empirical change rate coefficients for accretion (C^{+} for $\Delta E < 0$) and erosion (C^{-} for $\Delta E > 0$). The factor $E^{1/2}$ ensures small changes in *A* when *E* is small. The sign of *dA/dt* is determined by the sign of the energy disequilibrium,

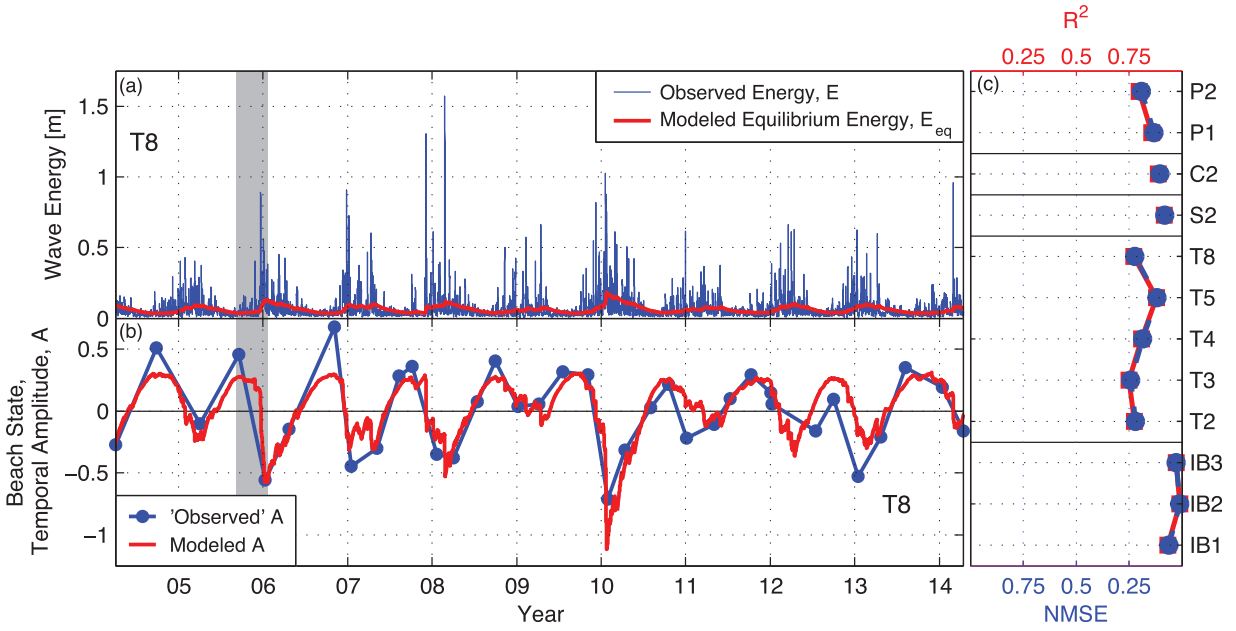

Figure 8. (a) Torrey Pines section T8 observed wave energy, E (blue), and modeled equilibrium wave energy, E_{eq} (red), versus time. (b) Observed (blue) and modeled (red) A (beach state) versus time at T8. When $E > E_{eq}$, the EOF temporal amplitude A decreases (the model beach face erodes and offshore bar accretes). When $E < E_{eq}$, A increases (beach face accretes and offshore bar erodes). Gray vertical bar is time period detailed in Figure 12. (c) Beach state model normalized mean square error (NMSE, blue) and skill (R^2, red and on top axis) versus sections well described by EOF 1. Modeled A has NMSE < 0.25 and $R^2 > 0.75$ at all modeled sections.

$$\Delta E = E - E_{eq}(A). \tag{2}$$

For simplicity, a linear equilibrium relationship is assumed,

$$E_{eq}(A) = aA + b, \tag{3}$$

where a and b are empirical parameters. For a given beach state, A, the equilibrium energy E_{eq} is the wave energy that causes no profile change. Rearranging (3) yields the equilibrium beach state for a given wave energy,

$$A_{eq} = \frac{E - b}{a}. \tag{4}$$

With constant E, the approach to equilibrium is exponential,

$$A(t) = (A_0 - A_{eq})\, e^{\left(-aC^{\pm}E^{1/2}t\right)} + A_{eq}, \tag{5}$$

where A_0 is the initial beach state, and $(A_0 - A_{eq})$ is the initial disequilibrium. The four free parameters, $C^{\pm}$, a, and b, are found as a best fit (minimum root-mean-square error (RMSE); Appendix A) between the observations and the model forced with hourly wave estimates. This nonlinear optimization problem is solved with simulated annealing [*Kirkpatrick and Vecchi*, 1983; *Barth and Wunsch*, 1990], a simple method that can navigate many local minima.

5.2. State Model Skill and Error

The equilibrium model for beach state, A, equations (1)–(3), was tested on the 12 beach sections where the first mode EOF well describes the profile observations (IB1, IB2, IB3, T2, T3, T4, T5, T8, S2, C2, P1, and P2). At T8, modeled and observed A are well correlated (Figure 8b), and at all sites $R^2 > 0.75$ and NMSE < 0.25 (Figure 8c). (Skill or R^2, and NMSE are defined in Appendix A.) Additional examples of modeled and observed A are in supporting information Figure S1. The model A error is consistently and anomalously large during the energetic El Niño winter 2009–2010 (Figure 9). Shoreface erosion (and offshore accretion) was overpredicted using model parameter values largely determined by more moderate conditions. The effect of varying the duration and intensity (e.g., including El Niño) of calibration periods on model performance is usually not strong, as discussed further below.

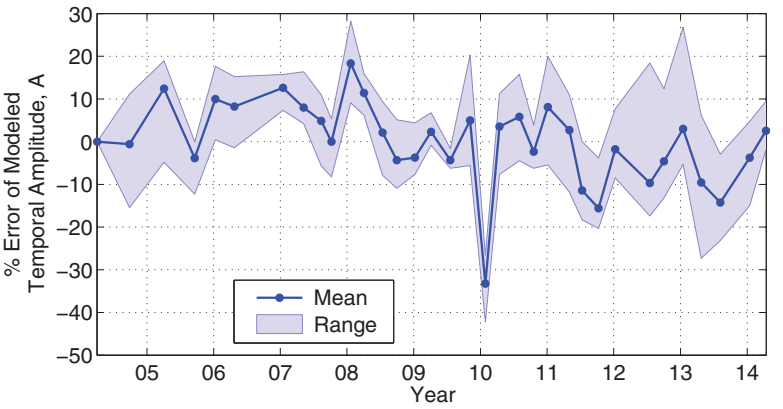

Figure 9. Percent error (Appendix A) in modeled beach state (temporal amplitude *A*) versus time. The percent error mean and range (see legend) are over the five sections at Torrey Pines (T2, T3, T4, T5, and T8) that are well described by EOF 1. Mean errors are extreme during the energetic 2010 El Niño; shoreline erosion and offshore accretion are overpredicted.

5.3. State Model Parameter Values and Transportability

Best fit model free parameters vary between sites (Figures 10a–10d). However, model performance is similar using a single set of parameters fit to all 12 sections (vertical dashed lines in Figures 10a–10d). The NMSE for the universal parameters is generally only slightly larger than with section-specific parameters (compare open circles with dark triangles in Figure 10e). As in *Yates et al.* [2009a, 2011] shoreline model, the free parameter values are not well constrained by the observations. For example, the horizontal bars in Figure 10d indicate the wide range of values for *a* for which the RMSE changes by less than 10% while holding other parameters constant. Furthermore, changes from optimal in one free parameter can be compensated by changes in other parameters such that the error minima in the four-dimensional parameter space are

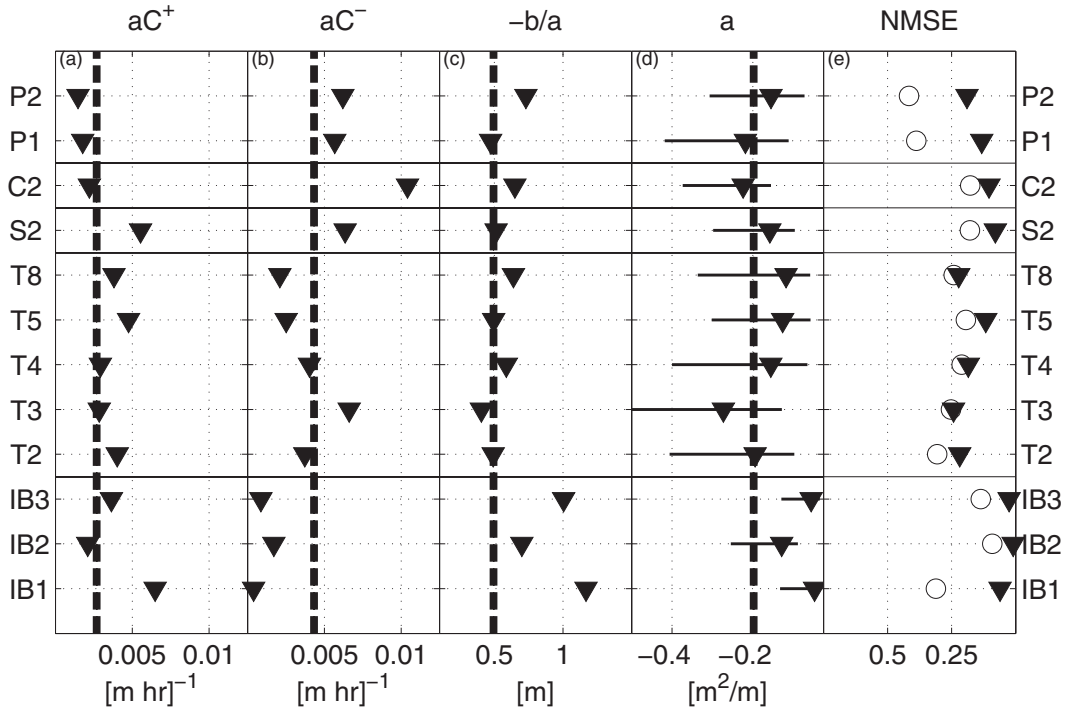

Figure 10. Optimal model free parameters and products: (a) aC^+, accretion *e*-folding scale coefficient; (b) aC^-, erosion *e*-folding scale coefficient; (c) $-b/a$, maximum beach state; (d) *a*, equilibrium slope. Results are shown for each individual section (triangles) and for all sections combined (dashed vertical lines). Horizontal lines in Figure 10d show range of values of *a* for which RMSE is increased by less than 10% while holding other parameters constant (parameters are not well constrained). (e) NMSE using free parameter values that are best fits for each individual section (solid triangles) and for all sections combined (open circles). Parameter *b* depends on the temporal mean removed from the time series and is not comparable between alongshore sections [*Yates et al.*, 2009a, 2011].

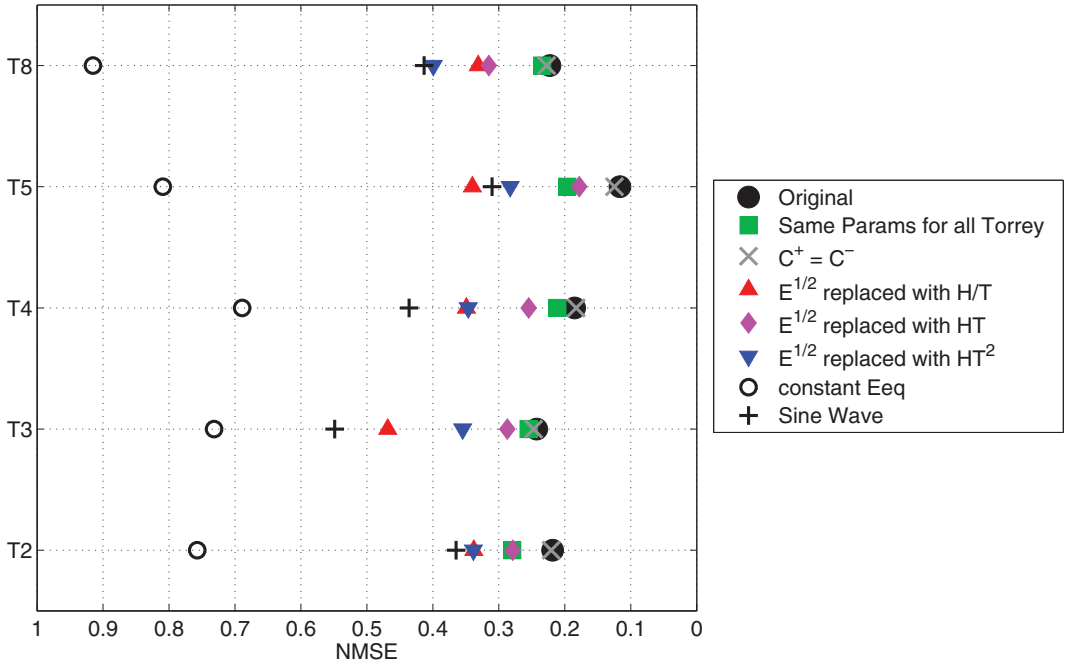

Figure 11. Modeled beach state NMSE (normalized mean square error) for Torrey Pines sections T2, T3, T4, T5, and T8, using different model formulations (see legend).

even more broad (not shown). Spatial variability in model parameter values has been ascribed to sand grain size and other physical factors [*Davidson et al*., 2013; *Splinter et al*., 2014; *Stokes et al*., 2015], but is only physically significant if the parameters are well constrained.

5.4. Alternative Beach State Model Formulations

Beach state model performance is relatively insensitive to details. For example, modeled beach state NMSE is increased only slightly by setting $C^+ = C^-$ and solving for three instead of four free parameters for each section at Torrey Pines (compare gray X with filled black circles in Figure 11). Using the same four optimal free parameters for all Torrey Pines sections also only slightly degrades results (green square in Figure 11). However, a constant E_{eq} significantly degrades model performance (open black circles in Figure 11) because the observed dependence of the beach state change rate on the present beach state (e.g., the variation of color along a line of constant $<E>$ in Figure 7a) is not modeled. Constant E_{eq} here is similar in principal to the constant $\Omega_{eq} = <H_b/(w_s T)>$ ($< >$ is time average) equilibrium condition used by *Davidson and Turner* [2009] and *Davidson et al*. [2010].

Model performance was insensitive to including wave period T in equation (1) when replacing $E^{1/2}$ (proportional to significant wave height H_s) with H_s/T, $H_s T$, and $H_s T^2$,

$$\frac{dA}{dt} = C^{\pm}\frac{H_s}{T}\left[\frac{H_s^2}{T^2} - (aA+b)\right], \tag{6}$$

$$\frac{dA}{dt} = C^{\pm}H_s T\left[H_s^2 T^2 - (aA+b)\right], \tag{7}$$

$$\frac{dA}{dt} = C^{\pm}H_s T^2\left[H_s^2 T^4 - (aA+b)\right], \tag{8}$$

where the parameters were recalibrated for each alternate formulation (Figure 11). *Yates et al*. [2009a] found their equilibrium shoreline model performed similarly for several formulations including replacing $E^{1/2}$ by E, E^2, the radiation stress component S_{xx}, or $\Omega = H_b/(w_s T)$ (H_b is the breaker height and w_s the sediment settling velocity). *Miller and Dean* [2004] showed that different rate proportionalities including H_b, H_b^2, H_b^3, or Ω were more effective at reproducing shoreline change at different beaches. *Davidson and Turner* [2009] and *Davidson et al*. [2010] employed Ω in their rate "forcing" term, while *Davidson et al*. [2013] and *Splinter*

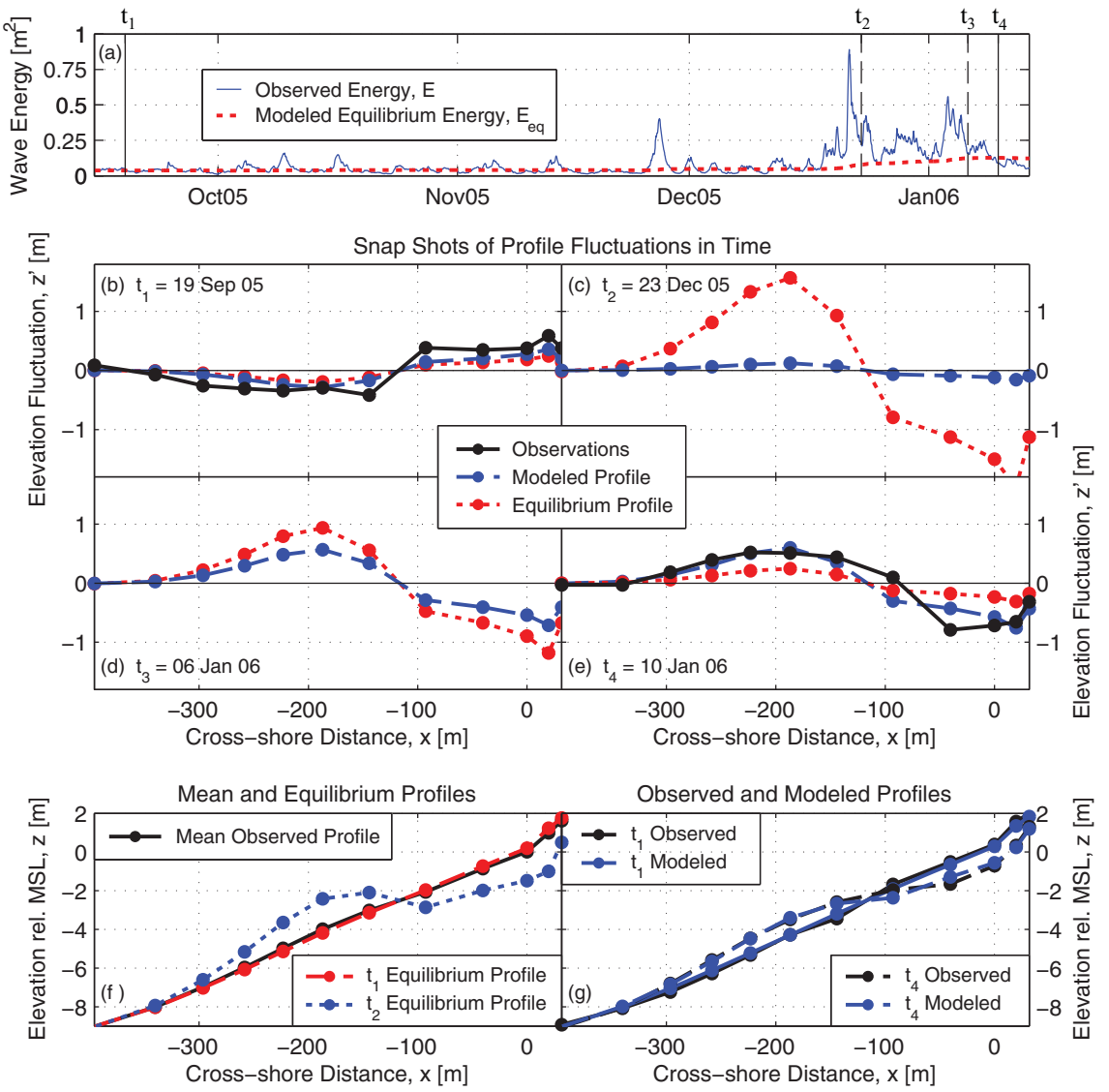

Figure 12. Torrey Pines section T8. (a) Observed and modeled equilibrium wave energy, E and E_{eq}, versus time for 4 months. Times t_1 through t_4 are labeled. (b–e) Modeled, observed (when available), and equilibrium profiles (demeaned) for times t_1 through t_4. The modeled profile (blue dashed) is evolving toward the equilibrium profile (red dotted) at each time step. (b) At t_1, the bermed beach is in equilibrium with the low E. (c) At t_2, the beach is out of equilibrium with the high E, and the beachface begins to erode while the offshore bar accretes. (d) By t_3, the barred beach is almost in equilibrium with the high E. (e) At t_4, E is low, and the barred beach begins to recover. Observations were acquired at t_1 and t_4 (black in Figures 12b and 12e). Elevation versus cross-shore distance for (f) mean and equilibrium profiles and (g) observed and modeled profiles.

et al. [2013, 2014] preferred a term proportional to $H\sqrt{T}$. *Davidson and Turner* [2009], *Davidson et al*. [2010, 2013], and *Splinter et al*. [2013, 2014] suggested Ω is an important parameter for modeling shoreline disequilibrium. Steeper waves (large H/T) may be more efficient at moving sediment, however *Stockdon et al*. [2006] suggests that runup at the shoreline during storms increases as HT^2, suggesting a drastically different dependence on wave period. Although almost certainly important to sediment transport, there is no data-based reason to include wave period in the present model. A simple sinusoidal three-parameter fit (amplitude, frequency, and phase) to the temporal amplitude provides a baseline (black cross in Figure 11) that is outperformed by all model versions except when E_{eq} is constant.

6. Discussion

6.1. Equilibrium Beach Profile Model

The first mode EOF demonstrates some skill at profile reconstruction (Figures 4e and 5b), and the first mode temporal amplitude A is well modeled at the selected sections (Figure 8c).

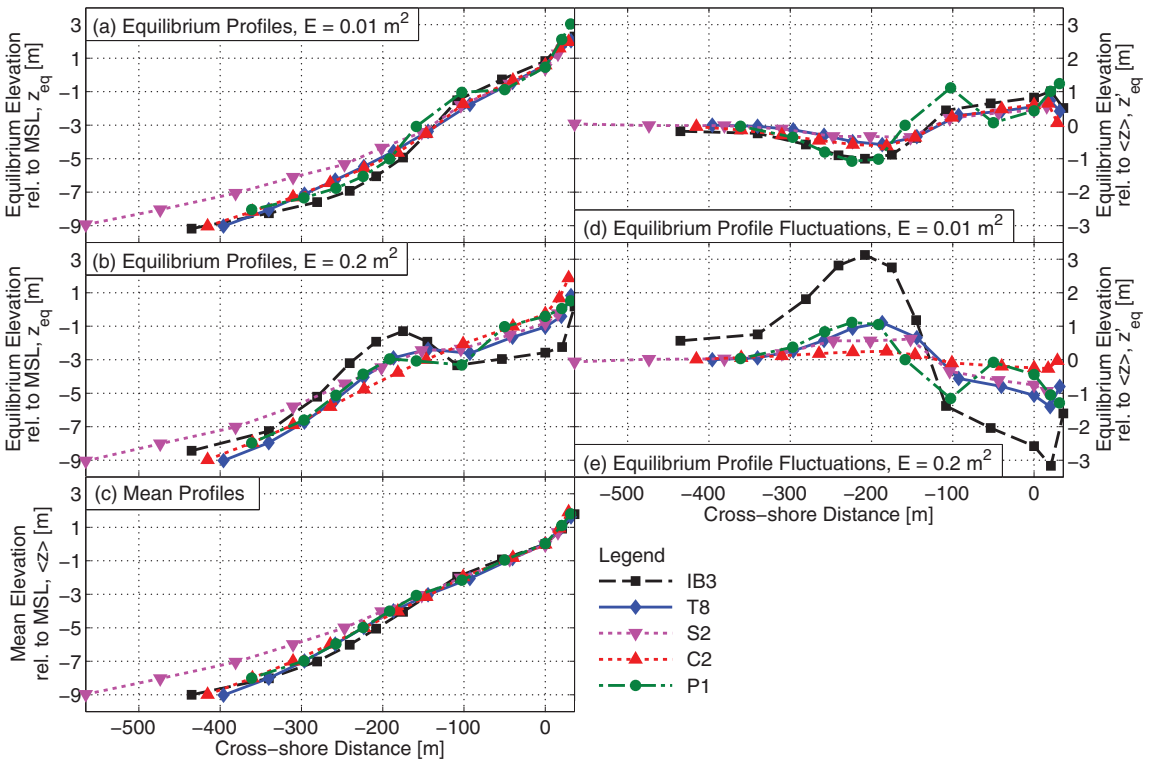

Figure 13. (a) Equilibrium beach profiles at sections representative of each beach site (see legend) for E = 0.01 m^2 (H_s = 0.4 m). (b) Same as Figure 13a but with E = 0.2 m^2 (H_s = 1.8 m). (c) Mean profiles. (d) Same as Figure 13a but with mean removed. (e) Same as Figure 13b but with mean removed.

6.1.1. Profile Model Formulation

As suggested by *Yates et al.* [2009a], the profile model uses the form of the first mode EOF reconstruction,

$$z(x,t) = W(x)A(t) + \langle z(x,t)\rangle, \tag{9}$$

where $\langle\rangle$ is the time mean, EOF analysis provides the spatial weights, W, and the temporal amplitude, A, is modeled with equilibrium equations (1)–(3). The profile model cannot outperform the skill of the first mode EOF reconstruction that it emulates. With N modeled cross-shore locations, W gives the $N-1$ additional empirical parameters that extend the state model to the profile ($W = 1$ at the shoreline). The equilibrium beach profile is calculated using equations (4) and (9),

$$z_{eq}(x,t) = W(x)\left(\frac{E(t)-b}{a}\right) + \langle z(x,t)\rangle. \tag{10}$$

Beach profile evolution at T8 for 4 months (period highlighted in gray in Figures 8 and 14) is shown in Figure 12. At the end of summer, the mildly bermed beach is in equilibrium (the blue dashed modeled profile is approximately the same as the red dotted equilibrium profile in Figure 12b) with the low E waves (19 September, time t_1, Figure 12a). For 2 months, E is low (Figure 12a), only briefly exceeds E_{eq}, and little beach change is predicted (not shown). With the higher energy waves between 18 December and 10 January, $E > E_{eq}$ (Figure 12a), the bermed beach is out of equilibrium (Figure 12c) and evolves toward a barred profile (Figure 12d). After E subsides at t_4, the barred beach is predicted to recover (Figure 12e).

Equilibrium profiles from all beach sites (shown in Figure 13 for low and moderate E = 0.01 m^2 and 0.2 m^2, H_s = 0.4 and 1.8 m, respectively) differ from the $x^{2/3}$ shape proposed by *Bruun* [1954] and others. Equilibrium profiles for higher E (not shown) often contain a nonphysically large offshore bar. However, the nonphysical bar is not predicted to develop for the field conditions, because high wave energy only persists briefly and equilibrium is not reached. For example at T8, with the present calibration, the offshore bar will exceed MSL if waves with E = 0.5 m^2 (H_s = 2.8 m) persist on an initially accreted profile of beach state $A = 1$ for longer than about 4.5 months. During the calibration period, waves only exceeded E = 0.5 m^2 during

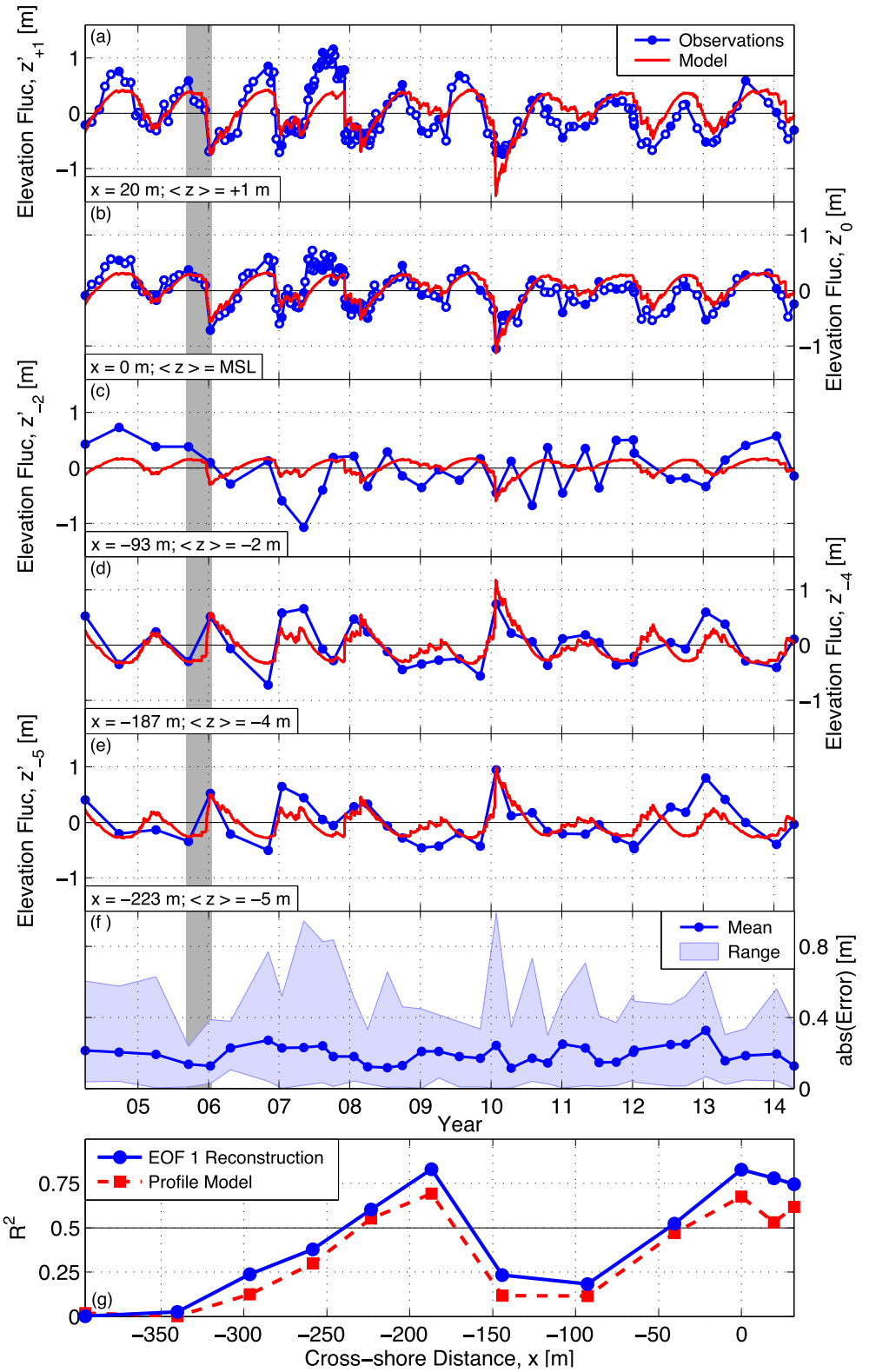

Figure 14. (a–e) Torrey Pines section T8 observed (blue curve with circles) and modeled (red) sand level fluctuations versus time. The mean sand elevations (see labels) range from (a) +1 m to (e) −5 m. Open blue circles in Figures 14a and 14b are subaerial surveys, not used in profile model calibration or evaluation. (f) Mean and range (see legend) of model misfit versus time. Gray bar is Figure 12 time period. (g) R^2 versus cross-shore distance. The profile model (red) works well ($R^2 > 0.5$) near the shoreline ($x = 0$) and in 4–5 m mean depth ($x = -200$ m), and generally follows the R^2 of the EOF reconstruction (blue curve is from Figure 4e). Additional errors from the imperfect modeling of the beach state, A (Figures 8b and 8c) are relatively small.

brief episodic storms (Figure 2d). The present model therefore cannot be extrapolated to periods of large waves much longer than used in the calibration. Given such observations, the profile model response can be calibrated and adjusted as necessary by altering equations (1)–(3).

6.1.2. Profile Model Skill and Error

Time series of modeled and observed sand elevations at various cross-shore locations are shown in Figures 14a–14e at T8. Note that the time series detailed in Figure 12 (shaded gray in Figures 8 and 14) is relatively well modeled with small absolute error (Figure 14f). Additional modeled and observed profiles are in supporting information Figure S2. Model error (Figure 14f) and skill (dashed red line with squares in Figure 14g) vary across the profile consistent with the performance of the first EOF mode reconstruction (solid blue line with circles in Figure 14g). Model skill is high near the shoreline (mean depths 0, +1 m) and at the typical winter bar location (mean depths −4 and −5 m). Offshore (mean depth −8 m), the skill is low, but changes are small (standard deviation in Figures 3 and 4e).

The model fails most significantly midprofile ($x = -100$ m), where skill is low (Figures 14c and 14g) and signal (standard deviation of observed elevations; Appendix A) is high (red dash-dotted curve in Figure 4e). Here the profile model fails because the EOF 1 reconstruction fails. EOF 1 reconstructs the data with a rocking motion, and the middepth profile tends to be at the node ($x = -125$ m, Figure 4b), so the model-

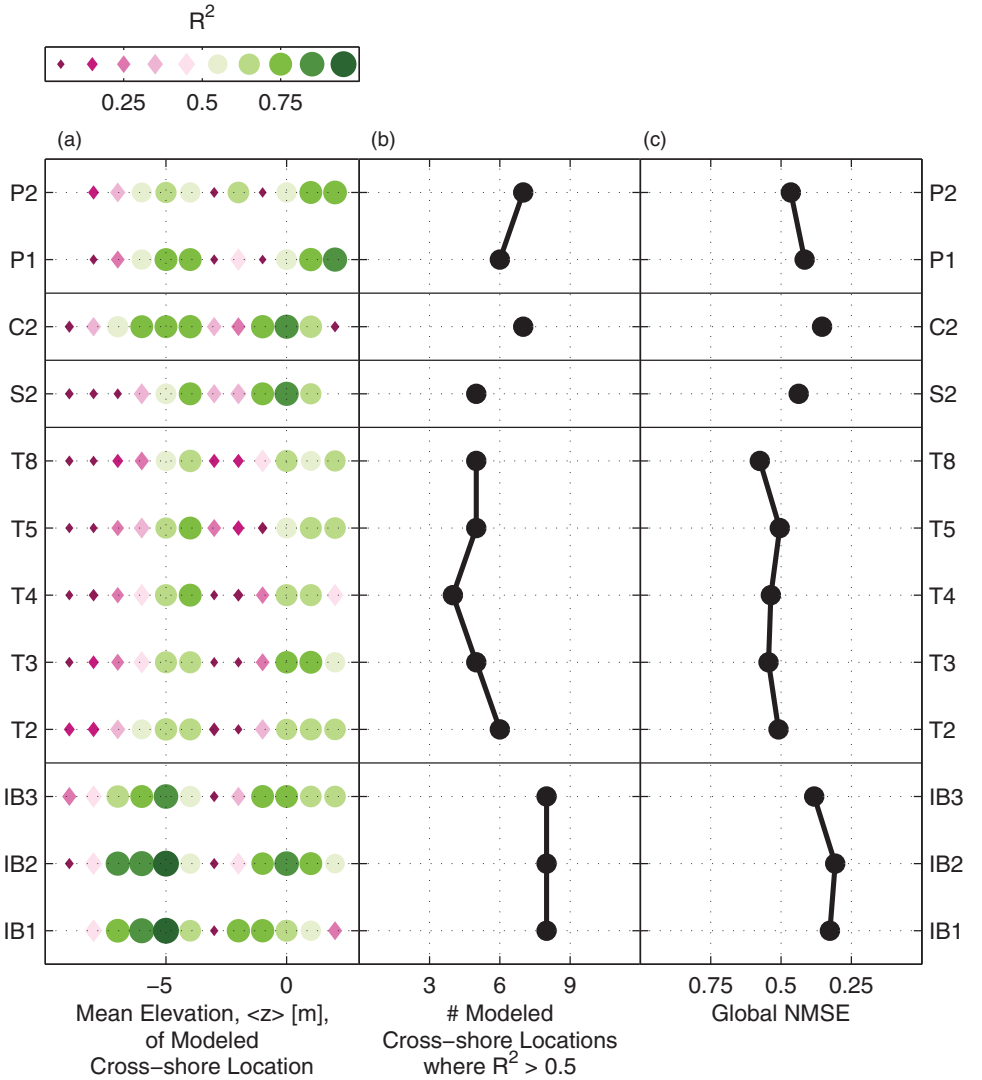

Figure 15. Profile model performance at the 12 modeled sections. (a) R^2 between observed and model sand level versus mean elevation and alongshore section (R^2 is coded by color and symbol, see bar at top). (b) Number of modeled cross-shore locations with total $R^2 > 0.5$. (c) Global NMSE (normalized mean square error).

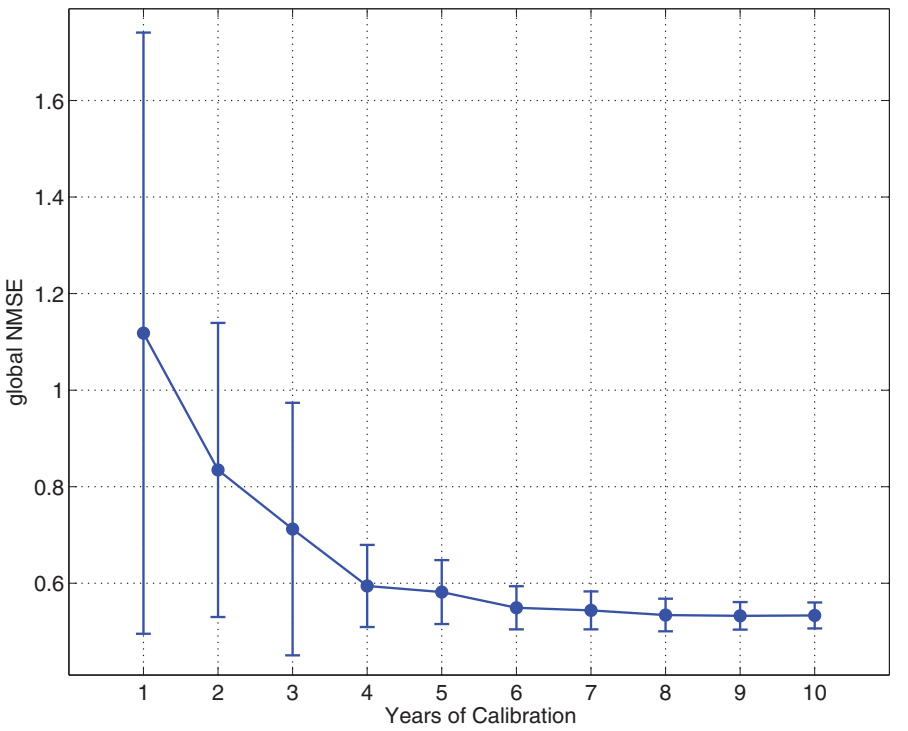

Figure 16. Beach profile model global NMSE versus years of parameter calibration. Standard deviation (scatter bars) includes variability from both different test periods and alongshore sections (T2, T3, T4, T5, and T8 are used). The number of cases for each years of calibration class is 1 year (50), 2 years (25), 3 years (15) tests, 4 years (10), 5 years (10), and 6, 7, 8, 9, and 10 years (5).

reconstructed elevation fluctuations are small (red in Figure 14c). Extending the equilibrium profile model equations (1)–(10) with EOF mode 2 or complex EOF mode 1 (CEOF 1) did not show promise for improving overall model performance (Appendix C).

The profile model performance is similar to T8 at all 12 sandy beach sections located away from significant sediment sources and sinks (Figure 15). The number of cross-shore locations with $R^2 > 0.5$ varies between 4 and 8 out of 11–12 (Figures 15a and 15b) and global NMSE < 0.6 (Figure 15c). Global NMSE is calculated by concatenating the time series at all cross-shore locations and calculating the NMSE (Appendix A).

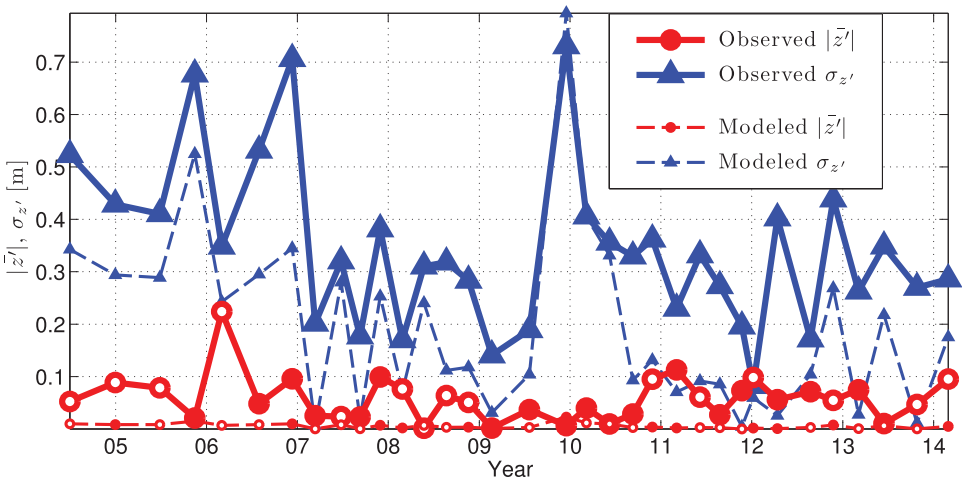

Figure 17. Equivalent sand level change versus time at T8. Curves are observed (solid) and modeled (dashed). Typically, the amount of sand exchanged between the bar and beach face (standard deviation of elevation change, $\sigma_{z'}$, triangles) is much larger than lost (or gained) integrated over the profile (mean change, $\overline{z'}$, circles, where absolute value is plotted with negative values shown as hollow circles).

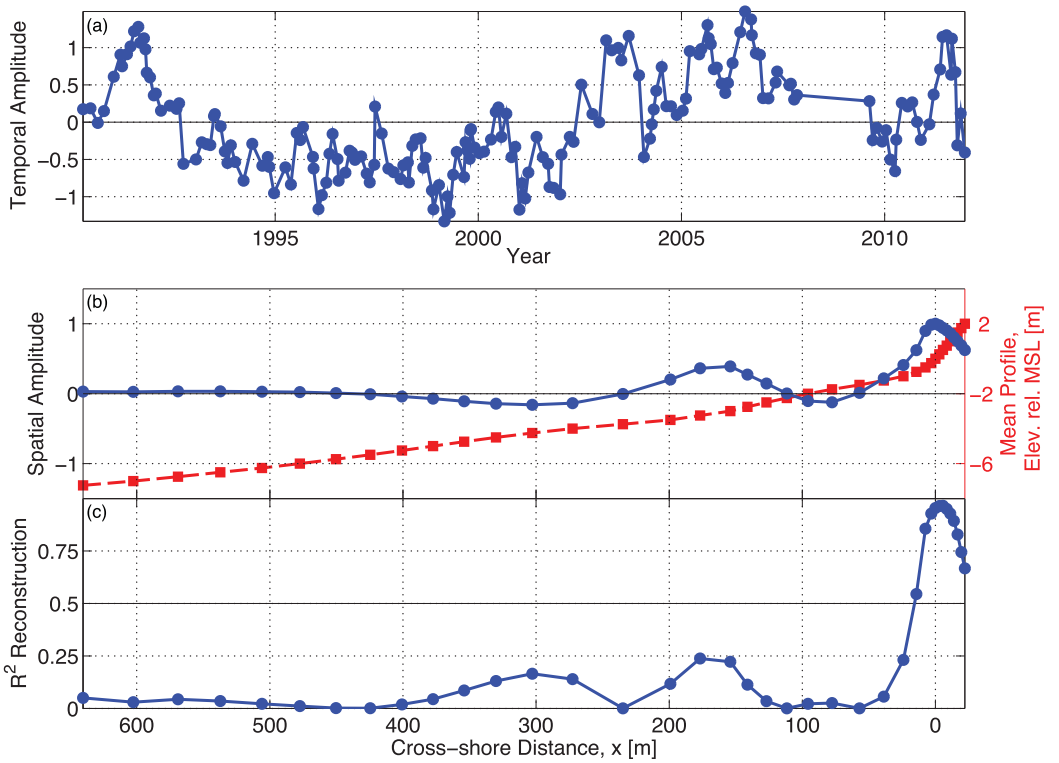

Figure 18. EOF 1 at Duck, south of the research pier. (a) Temporal amplitude. (b) Spatial amplitude (solid blue curve with circles, left axis) and mean profile (dashed red curve with squares, right axis). (c) R^2 of reconstruction shows the first mode only well describes the upper beach; changes in the rest of the profile are incoherent with the upper beach. Analysis of various alongshore subsections and over the entire reach at Duck all yield similar results.

6.1.3. Profile Model Calibration Duration

Profile model performance changes with calibration duration (Figure 16). Both the beach state parameters, a, b, and $C^{\pm}$, determined by optimization, and the spatial shape function parameters, $W(x)$, determined by EOF analysis, are considered in the calibration. With 1 year of calibration, global NMSE is close to 1, so the prediction is not better than predicting the mean profile. Global NMSE decreases with 2 and 3 years of calibration, but then flattens out, qualitatively similar to the results for shoreline model calibrations [*Yates et al.*, 2009a; *Splinter et al.*, 2013]. Including the El Niño winter in the calibration period reduces errors during El Niño, but slightly degrades model performance for the rest of the time series (not shown).

6.1.4. Nonconservation of Mass

The cross-shore integrated difference between successive transects does not sum to zero, either in the observations or model. Mass on a transect is not conserved. The elevation fluctuation (Figures 12b–12e) of each observed and modeled profile is interpolated to a uniformly spaced cross-shore grid. The equivalent thickness is the cross-shore average of the interpolated elevation fluctuation, $\overline{z'}$ at each observed or modeled survey. An equivalent thickness of a uniform layer over the transect, $\overline{z'}$, is usually $<|10|$ cm at T8 (solid curve with large red circles in Figure 17), approximately the expected GPS bias error. Mass is less conserved at some other sections, and equivalent $\overline{z'}$ of 20–30 cm, larger than the likely measurement errors, are not uncommon. The model $\overline{z'}$ (dashed curve with small red circles in Figure 17) can also reach 20–30 cm (not shown) but tends to be much smaller and noisy, and fails to simulate observed changes in mass on a transect. In contrast, the model better reproduces the larger $\sigma_{z'}$, the standard deviation of the elevation fluctuation across the profile at each survey (between about 10 and 70 cm, blue curves with triangles in Figure 17). Modeled $\sigma_{z'}$ are smaller than observed $\sigma_{z'}$, because only spatially coherent fluctuations are modeled.

6.1.5. Changing Water Levels

Southern California water levels are dominated by tides with spring elevation changes up to 2.7 m. Storm surge is usually small, although wave-induced setup can raise water levels by more than a meter [*Flick and Badan-Dangon*, 1989], and El Niño events may raise water levels as much as 30 cm. The timing of wave

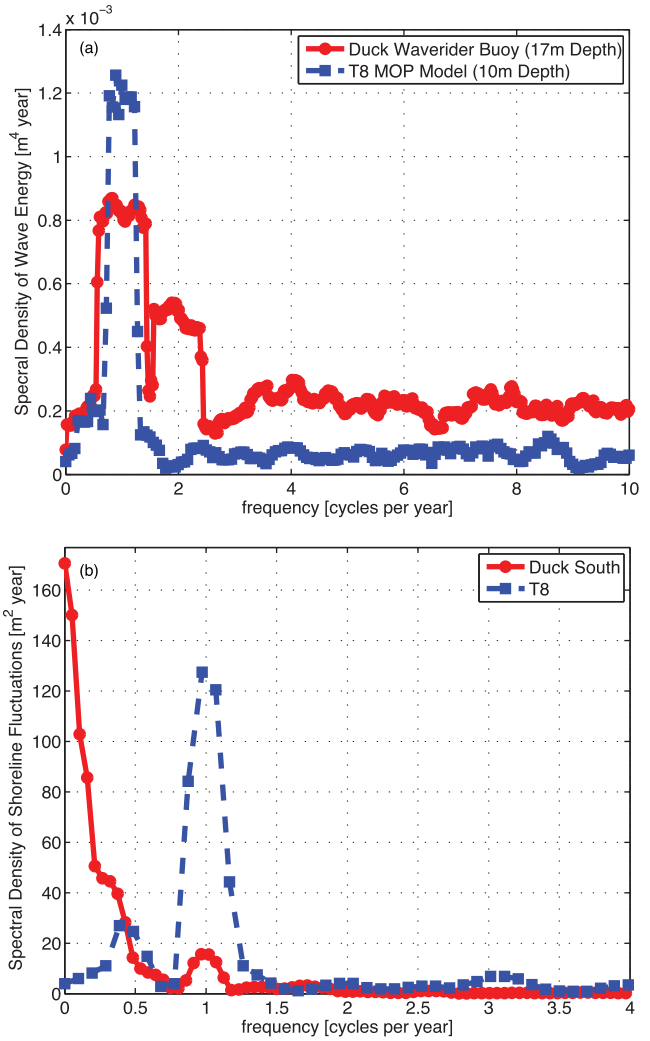

Figure 19. (a) Wave energy spectra of Duck waverider buoy (red solid line with circles) and T8 MOP model (blue dashed line with squares). Both have energetic peaks at the annual frequency. (b) Shoreline elevation fluctuation spectra at Duck (south of the pier) and T8. Torrey shoreline fluctuations have a strong annual signal but the Duck shoreline is dominated by low-frequency variability.

events relative to water level can be important for profile change [*Coco et al.*, 2014]. Here the EOF-derived profile weights $W(x)$ allow the upper profile to move even if it is not wet. Observations with higher time resolution, that resolve changes with tidal level during storms, are needed to develop and test an equilibrium profile model extended to include changing water levels. A model modified to include variable water levels could use a coordinate origin ($x = 0$) that varies with water level (similar to *Bruun* [1962] and discussed conceptually in *Castelle et al.* [2014]), rather than the location of the shoreline on the average profile used here.

6.2. Model Failure at Duck, NC

Shoreline equilibrium models succeed at beaches with a range of morphologies including multibarred beaches with alongshore variations [*Miller and Dean*, 2004; *Davidson et al.*, 2013; *Splinter et al.*, 2013, 2014; *Castelle et al.*, 2014], but fail at the alongshore nonuniform multibarred Duck Beach, NC [*Miller and Dean*, 2004; *Splinter et al.*, 2014]. The present *profile* model also fails. The profile model depends fundamentally on spatially coherent fluctuations across the profile, yet only locations with mean depths 0, 1, and 2 m are described well by the first EOF at Duck (Figure 18c). This contrasts with the southern California beaches, where offshore and near-shoreline locations are strongly coupled. In addition, the amplitude function A (Figure 18a) varies at longer than annual time scales and does not follow the present equilibrium framework (not shown). Even when averaging over longer alongshore spans and band passing to isolate the small annual signal, the Duck profile was not equilibrium like according to the present model (not shown). *Plant et al.* [1999, 2001] showed that bars at Duck migrate toward an equilibrium location. Complex EOFs (CEOFs) better reconstruct the Duck observations [*Ruessink*, 2003] and their potential application in an equilibrium profile model similar to the bar crest position model of *Plant et al.* [1999] is discussed in Appendix C.

The reasons for the dramatically different profile evolution at Duck and southern California are unknown. Although the Duck wavefield is seasonal, similar to southern California (Figure 19a), the shoreline and other cross-shore locations (not shown) have a small annual signal, and are dominated by lower frequencies (Figure 19b) [*Plant et al.*, 1999; *Pianca et al.*, 2015]. The evolution of complex two-dimensional morphology (e.g., bar attachment, detachment, and straightening) has been studied extensively at several beaches, including

Duck [*Lippmann and Holman*, 1990; *Holland*, 1998; *Konicki and Holman*, 2000; *Plant et al*., 2006]. The research pier also induces alongshore variations [*Plant et al*., 1999; *Pianca et al*., 2015]. Perhaps, even when alongshore averaged (with or without the vicinity of the pier excluded), these 2-D bar-dominated morphologies are fundamentally different than southern California. The steep foreshore, cross-shore variations in grain size, and exposure to hurricanes and Nor'easters at Duck may also play a role [*Larson and Kraus*, 1994; *Plant et al*., 1999; *Pianca et al*., 2015].

7. Summary and Conclusions

EOF analysis of profile evolution shows (consistent with previous work) that sandy southern California beaches located away from significant sediment sources and sinks exhibit an annual cross-shore rocking behavior, where the profile adjusts from barred in winter to bermed in summer. At these 12 (of 19) well-behaved sections, the temporal amplitude A of the first mode EOF is a measure of beach profile state. The observations suggest beach state change rate dA/dt depends on both incident wave energy and the present beach state. This is consistent with the equilibrium hypothesis; there is an equilibrium profile for every incident wave condition, and the profile evolves toward equilibrium at a rate proportional to the disequilibrium: the distance from the present to the equilibrium state. The same moderate wave conditions will erode an already accreted beach face (creating an offshore bar), and accrete an already eroded beach face.

A simple beach state model, driven by hourly wave energy, is used to quantify the equilibrium hypothesis at the 12 sections well described by the first EOF. The three or four parameter beach state model for A has high skill ($R^2 > 0.75$), although the model free parameters are not well constrained. Globally optimized parameters perform almost as well as section-specific values. The beach state model is extended to describe the profile using the spatial weights of the first EOF. The EOF-based equilibrium beach profile differs from the classic $x^{2/3}$ profile. The profile model has high skill where the EOF reconstruction is also skillful and fails where the EOF reconstruction fails, most notably at middepths. After a few years of calibration with quarterly observations, skill does not increase with longer calibration. The model overpredicts shoreline erosion and offshore accretion during the anomalously energetic storms of the El Niño 2010, and cannot be extrapolated for use in persistent large wave conditions. Increasing the equilibrium model complexity may be problematic because equally plausible modifications to the somewhat arbitrary modeling assumptions can yield similar (or no improvement in) model performance. The equilibrium profile model is crude and simplistic and does not necessarily conserve mass or momentum. It does reproduce selected observations well (using empirical parameters), supports the equilibrium hypothesis, and provides a baseline skill level for comparable predictions by physics-based process models. Physics-based process models are needed to quantify the complex fluid and sediment dynamics underlying the observed macroscopic equilibrium behavior, to determine the role of the neglected alongshore transport, and to explore causes of model failure.

Appendix A: Statistical Definitions

With fluctuation $x' = x - \langle x \rangle$, where $\langle x \rangle$ is mean, definitions are,

$$\text{Standard deviation: } \sigma_x = \sqrt{\langle x'^2 \rangle}, \tag{A1}$$

$$\text{Skill: } R^2 = \frac{\langle x'y' \rangle^2}{\sigma_x^2 \sigma_y^2}, \tag{A2}$$

$$\text{Root-mean-square error: RMSE} = \sqrt{\langle (y-x)^2 \rangle}, \tag{A3}$$

$$\text{Normalized mean square error: NMSE} = \frac{\langle (y-x)^2 \rangle}{\sigma_x^2}, \tag{A4}$$

$$\text{Percent error: \% error} = 100 \frac{y-x}{\max(x) - \min(x)}. \tag{A5}$$

Appendix B: EOF Analysis Method

The data set is decomposed with standard methods as

$$\vec{z'}(t)=\sum_{i=1}^{N} A_i(t)\vec{w}_i, \tag{B1}$$

where $\vec{w}_i$ are orthonormal basis vectors (EOFs),

$$\vec{w}_i^T\vec{w}_j=\delta_{ij}, \tag{B2}$$

with length N (the number of spatial locations). The temporal amplitudes

$$A_i=\vec{w}_i^T\vec{z'}, \tag{B3}$$

are also orthogonal

$$\langle A_iA_j\rangle=\delta_{ij}\langle A_i^2\rangle. \tag{B4}$$

With $\vec{W}$ a matrix with columns of the basis vectors $\vec{w}_i$, and $\vec{D}$ a diagonal matrix with elements equal to the variance of each A_i, (B1) is rewritten as the eigenvalue problem

$$\langle\vec{z'}\vec{z'}^T\rangle\vec{W}=\vec{W}\vec{D}, \tag{B5}$$

where the diagonal of $\vec{D}$ are the eigenvalues, and columns of $\vec{W}$ are the eigenvectors, or EOFs. The EOF eigenvalue problem is solved with a singular decomposition [*Kelly*, 1988] and uses the convention that spatial weight $\vec{w}_i=1$ at the average shoreline position, $x=0$. The first mode reconstruction, $A_1\vec{w}_1$, explains the most variance in the data set. Here A and W refer to the first mode A_1 and $\vec{w}_1$, respectively, unless otherwise specified.

Appendix C: EOF Mode 2 and CEOF Mode 1

The profile model has poor skill at middepths and offshore because the first EOF does not well reconstruct the profile at these locations (Figures 4e, 5b, 14g, and 15a). Vertical fluctuations at the deeper locations are small and relatively noisy. At middepths, however, the elevation fluctuations are large (Figures 3 and 4e). The node of the EOF 1 standing wave is at the poorly modeled middepth part of the profile (Figures 4b and 4e, blue solid line in Figures C1b and C1c). If elevation changes are best described by a propagating wave, at least two EOF standing wave modes, or one CEOF mode would be necessary to describe the profile evolution. We explored the behavior of EOF mode 2 and complex EOF (CEOF) mode 1 for ways to extend the EOF mode 1-based equilibrium profile framework, but these modes did not show promise for improving overall model skill in southern California.

While EOF 2 does have large spatial amplitude (red dashed line in Figure C1b) and some skill at middepths (red dashed line in Figure C1c), the temporal amplitude does not behave in a manner consistent with well-organized cross-shore propagation (red dashed line in Figure C1a) for which we expect the EOF 2 temporal amplitude (with positive spatial amplitude at middepth) to be large and positive where EOF 1 temporal amplitude is near zero (compare blue solid and red dashed lines in Figure C1a). (Similarly, we would expect EOF 2 temporal amplitude to be large and negative where EOF 1 temporal amplitude is extreme.) This is not the case.

CEOF analysis [*Horel*, 1984] has been widely used to study sandbar migration, notably *Ruessink* [2003]. CEOF analysis is performed in the same manner as traditional EOF analysis (Appendix B) except that $\vec{z'}$ is replaced by $\tilde{z'}$,

$$\tilde{z'}=\vec{z'}+iH\left\{\vec{z'}\right\}, \tag{C1}$$

where H is the Hilbert transform. By considering only the first mode, which again explains the majority of the variance in the observations, an approximation for $\vec{z}$ is recovered,

$$\vec{z'}(x,t)\approx M(x)V(t)\cos\left[\theta(x)-\psi(t)\right], \tag{C2}$$

where $M(x)$ is the spatial envelope of the bar amplitude, $V(t)$ represents the normalized temporal variations in $M(x)$, and $\theta(x)$ and $\psi(t)$ are the spatial and temporal phase, respectively. $M(x)$ (thick black line, left axis in

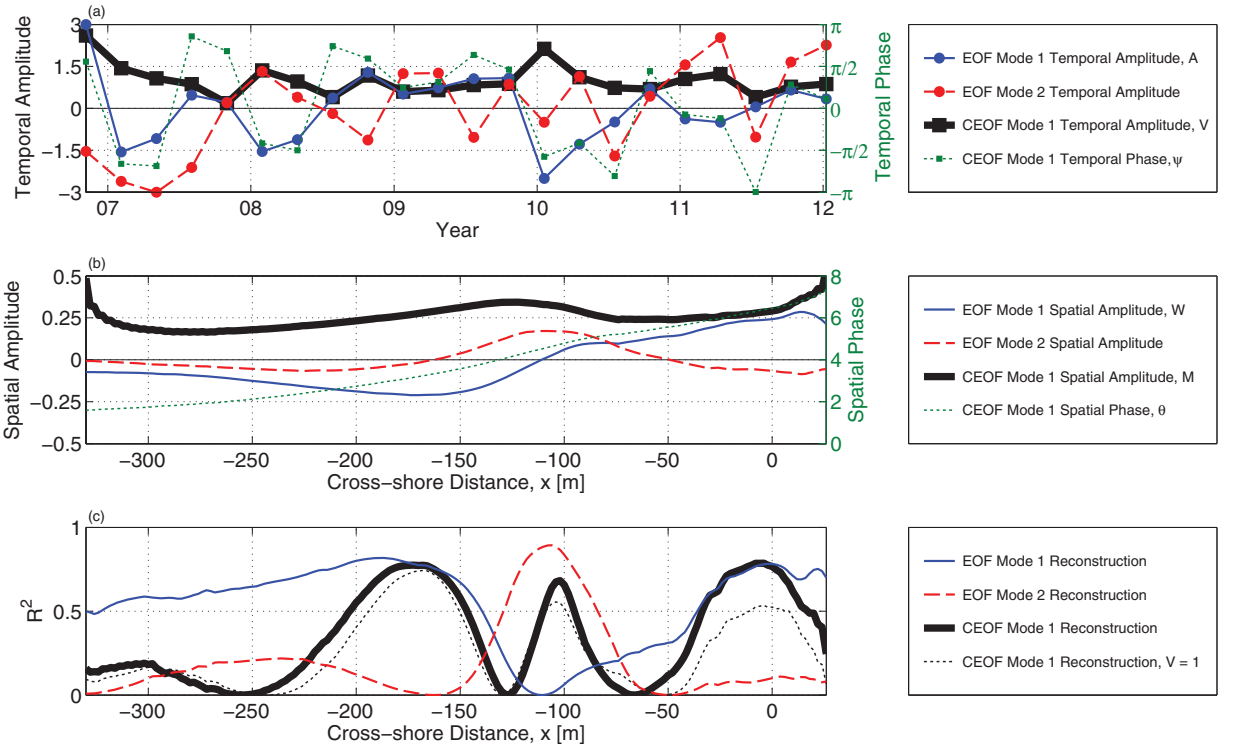

Figure C1. EOF modes 1 and 2 and CEOF mode 1 at T8. (a) Temporal amplitude (and CEOF temporal phase, right axis) versus time. (b) Spatial amplitude (and unwrapped CEOF spatial phase, right axis) versus cross-shore distance. (c) R^2 of the reconstruction versus cross-shore distance. The dotted black line shows CEOF 1 reconstruction skill when V (thick black line in Figure C1a) is forced to equal 1.

Figure C1b) and $V(t)$ (thick black line, left axis in Figure C1a) are the absolute values of the now complex first mode spatial eigenfunction, W, and temporal amplitude, A, respectively. Spatial phase θ (thin green line, right axis in Figure C1b) and temporal phase ψ (thin green line, right axis in Figure C1a) are defined as,

$$\theta(x)=\arctan\left[\frac{\Im\{W(x)\}}{\Re\{W(x)\}}\right], \tag{C3}$$

$$\psi(x)=\arctan\left[\frac{\Im\{A(t)\}}{\Re\{A(t)\}}\right], \tag{C4}$$

where $\Re\{\}$ and $\Im\{\}$ denote real and imaginary parts, respectively. Bar length is defined as,

$$L(x)=\frac{2\pi}{\Delta\theta(x)}. \tag{C5}$$

Time periods with relatively high temporal and spatial resolution at T2, T3, T4, T5, and T8 were used to compare EOF mode 1 and 2 to CEOF mode 1 in southern California. These observations were interpolated to uniformly spaced spatial and temporal grids. At T8, EOF modes 1 and 2 explain 54% and 21% of the data variance, respectively, while CEOF mode 1 explains 70%. Compared with the barred beaches in *Ruessink* [2003], CEOF 1 temporal amplitude variations are large (Figure C1a), spatial amplitude is small (Figure C1b), and the reconstruction does not describe a large unbroken region of the profile (R^2 is fairly low, Figure C1c). Bar length (not shown) is noisy except around $x=-150$ to -100 m (mean depth ~2–3 m) where $L(x)\sim 250$ m, consistent with *Ruessink* [2003].

A possible way to extend the equilibrium framework by using the first CEOF is to assume that the temporal magnitude is constant and temporal phase is equilibrium like. The dotted line in Figure C1c shows how CEOF 1 reconstruction skill is further degraded by assuming the temporal magnitude is constant. After this simplification, CEOF 1 is not a much better reconstruction than EOF 1. Furthermore, the temporal phase is only slightly correlated with the equilibrium-like EOF 1 temporal amplitude (Figure C1a). For these reasons, we

prefer the EOF model formulation in southern California. A CEOF-based equilibrium profile model of this sort would be similar to the bar crest position model of *Plant et al.* [1999] and *Pape et al.* [2010] and would likely be more suited for the barred beaches similar to those described in *Ruessink* [2003] including Duck, NC.

Acknowledgments
Imperial and Cardiff Beach sand level data are available at http://cdip.ucsd.edu/SCBPS/regions/, and observations from the other southern California beach sites will be posted here in accordance with the AGU data policy. Southern California bathymetry and wave data collection were supported by the United States Army Corps of Engineers and the California Department of Parks and Recreation Division of Boating and Waterways (program manager Reinhard Flick). Bonnie Ludka was partially supported by a National Science Foundation Graduate Research Fellowship, NOAA grant NA10OAR4170060, and California Sea grant project #R/RCC-01, through NOAA's National Sea Grant College Program, NOAA/Southern California Coastal Ocean and Observing System, United States Army Corps of Engineers and California Department of Parks and Recreation. The statements, findings, conclusions and recommendations are those of the authors and do not necessarily reflect the views of the aforementioned organizations. Kathleen Ritzman, Scripps Institution of Oceanography Assistant Director, was instrumental in maintaining funding and survey continuity for the Southern California monitoring program. Brian Woodward, Kent Smith, Dennis Darnell, Bill Boyd, Rob Grenzeback, Ian Nagy, and Zoe Dagan built and maintained the surveying system and have collected more than 380 beach elevation surveys. The Coastal Data Information Program (manager Julie Thomas) maintained and operated the wave network. Michele Okihiro coordinated permits and logistics. Lifeguard Captain Robert Stabenow ensured safe access to Imperial Beach. It took a village to raise this data set. Thank you. Jesse McNinch and the U.S. Army Corps of Engineers Field Research Facility generously provided all Duck, NC data.

References

Aubrey, D. G. (1979), Seasonal patterns of onshore/offshore sediment movement, *J. Geophys. Res.*, *84*(C10), 6347–6354.
Aubrey, D. G., D. L. Inman, and C. D. Winant (1980), The statistical prediction of beach changes in southern California, *J. Geophys. Res.*, *85*(C6), 3264–3276.
Bakker, W. T. (1968), The dynamics of a coast with a groin system, paper presented at 11th Conference on Coastal Engineering, ASCE, London, U. K.
Barth, N., and C. Wunsch (1990), Oceanographic experiment design by simulated annealing, *J. Phys. Oceanogr.*, *20*(9), 1249–1263.
Bruun, P. (1954), Coastal erosion and development of beach profiles, *Tech. Rep. Memo 44*, U. S. Army Corps of Eng., Washington, D. C.
Bruun, P. (1962), Sea level rise as a cause of shore erosion, *J. Waterw. Harbors Coastal Eng. Div. Am. Soc. Civ. Eng.*, *88*, 117–130.
Callaghan, D. P., R. Ranasinghe, and D. Roelvink (2013), Probabilistic estimation of storm erosion using analytical, semi-empirical, and process based storm erosion models, *Coastal Eng.*, *82*, 64–75.
Castelle, B., V. Marieu, S. Bujan, S. Ferreira, J.-P. Parisot, S. Capo, N. Sénéchal, and T. Chouzenoux (2014), Equilibrium shoreline modelling of a high-energy meso-macrotidal multiple-barred beach, *Mar. Geol.*, *347*, 85–94.
Coco, G., N. Senechal, A. Rejas, K. R. Bryan, and S. Capo (2014), Beach response to a sequence of extreme storms, *Geomorphology*, *204*, 493–501.
Davidson, M. A., and I. L. Turner (2009), A behavioral template beach profile model for predicting seasonal to interannual shoreline evolution, *J. Geophys. Res.*, *114*, F01020, doi:10.1029/2007JF000888.
Davidson, M. A., R. P. Lewis, and I. L. Turner (2010), Forecasting seasonal to multi-year shoreline change, *Coastal Eng.*, *57*, 620–629.
Davidson, M. A., K. D. Splinter, and I. L. Turner (2013), A simple equilibrium model for predicting shoreline change, *Coastal Eng.*, *73*, 191–202.
Davis, R. E. (1976), Predictability of sea surface temperature and sea level pressure anomalies over the North Pacific Ocean, *J. Phys. Oceanogr.*, *6*(3), 249–266.
Dean, R. G. (1991), Equilibrium beach profiles: Characteristics and applications, *J. Coastal Res.*, *7*(1), 53–84.
Dubarbier, B., B. Castelle, B. Marieu, and B. G. Ruessink (2015), Process-based modelling of cross-shore sandbar behaviour, *Coastal Eng.*, *95*, 35–50.
Flick, R. E., and A. Badan-Dangon (1989), Coastal sea levels during the January 1988 storm off the California, *Shore Beach*, *57*(4), 28–31.
Gallagher, E. L., S. Elgar, and R. T. Guza (1998), Observations of sand bar evolution on a natural beach, *J. Geophys. Res.*, *103*(C2), 3203–3215.
Haas, J. K. (2005), Grain size and mineralogical characteristics of beach sand in the Oceanside Littoral Cell, Southern California: Implications for sediment provenance, MS thesis, Univ. of Calif., San Diego.
Hoefel, F., and S. Elgar (2003), Wave induced sediment transport and sandbar migration, *Science*, *299*(5614), 1885–1887.
Holland, K. T. (1998), Beach cusp formation and spacings at Duck, USA, *Cont. Shelf Res.*, *18*(10), 1081–1098.
Holman, R. A., D. M. Lalejini, K. Edwards, and J. Veeramony (2014), A parametric model for barred equilibrium beach profiles, *Coastal Eng.*, *90*, 85–94.
Horel, J. D. (1984), Complex principal component analysis: Theory and examples, *J. Clim. Appl. Meteorol.*, *23*(12), 1660–1673.
Inman, D. L. (1953), Areal and seasonal variations in beach and nearshore sediments at La Jolla, California, *Tech. Rep. Memo 39*, Beach Erosion Board, U. S. Army Corps of Eng., Washington, D. C.
Inman, D. L., and G. A. Rusnak (1956), Changes in sand level on the beach and shelf at La Jolla, California, *Tech. Rep. Memo 82*, Beach Erosion Board, U. S. Army Corps of Eng., Washington, D. C.
Kelly, K. A. (1988), Comment on "Empirical orthogonal function analysis of advanced very high resolution radiometer surface temperature patterns in Santa Barbara Channel" by GSE Lagerloef and RL Bernstein, *J. Geophys. Res.*, *93*(C12), 15,753–15,754.
Kirkpatrick, S., and M. P. Vecchi (1983), Optimization by simulated annealing, *Science*, *220*(4598), 671–680.
Konicki, K. M., and R. A. Holman (2000), The statistics and kinematics of transverse sand bars on an open coast, *Mar. Geol.*, *169*(1), 69–101.
Kriebel, D. L., and R. G. Dean (1985), Numerical simulation of time-dependent beach and dune erosion, *Coastal Eng.*, *9*(3), 221–245.
Kriebel, D. L., and R. G. Dean (1993), Convolution method for time dependent beach profile response, *J. Waterw. Port Coastal Ocean Eng.*, *119*, 204–226.
Kuriyama, Y. (2012), Process-based one-dimensional model for cyclic longshore bar evolution, *Coastal Eng.*, *62*, 48–61.
Larson, M., and N. C. Kraus (1989), SBEACH: Numerical model for simulating storm-induced beach change, *Tech. Rep. CERC-89-9*, U. S. Army Corps of Eng., Vicksburg, Miss.
Larson, M., and N. C. Kraus (1994), Temporal and spatial scales of beach profile change, Duck, North Carolina, *Mar. Geol.*, *117*(1), 75–94.
Larson, M., M. Capobianco, and H. Hanson (2000), Relationship between beach profiles and waves at Duck, North Carolina, determined by canonical correlation analysis, *Mar. Geol.*, *163*(1–4), 275–288.
Lippmann, T. C., and R. A. Holman (1990), The spatial and temporal variability of sand bar morphology, *J. Geophys. Res.*, *95*(C7), 11,575–11,590.
Lorenz, E. N. (1956), Empirical orthogonal functions and statistical weather prediction, *Tech. Rep. 1*, Dep. of Meteorol., Mass. Inst. of Technol., Cambridge, Mass.
McCall, R. T., J. S. M. Van Thiel de Vries, N. G. Plant, A. R. Van Dongeren, J. A. Roelvink, D. M. Thompson, and A. J. H. M. Reniers (2010), Two-dimensional time dependent hurricane overwash and erosion modeling at Santa Rosa Island, *Coastal Eng.*, *57*(7), 668–683.
McGranahan, G., D. Balk, and B. Anderson (2007), The rising tide: Assessing the risks of climate change and human settlements in low elevation coastal zones, *Environ. Urbanization*, *19*(1), 17–37.
Miller, J. K., and R. G. Dean (2004), A simple new shoreline change model, *Coastal Eng.*, *51*(7), 531–556.
Moffatt and Nichol (2010), Coastal regional sediment management plan for the San Diego region, Tech. Rep. 6731-01, SANDAG, Long Beach, Calif.
O'Reilly, W. C., and R. T. Guza (1998), Assimilating coastal wave observations in regional swell predictions. Part I: Inverse methods, *J. Phys. Oceanogr.*, *28*(4), 679–691.
Pape, L., N. G. Plant, and B. G. Ruessink (2010), On cross-shore migration and equilibrium states of nearshore sandbars, *J. Geophys. Res.*, *115*, F03008, doi:10.1029/2009JF001501.
Pawka, S. S. (1983), Island shadows in wave directional spectra, *J. Geophys. Res.*, *88*(C4), 2579–2591.
Pelnard-Considére, R. (1956), Essai de theorie de l'evolution des formes de rivage en plages de sable et de galets, in *4th Journees de l'Hydraulique, Les Energies de la Mer, Paris*, vol. III-1, pp. 289–298, Soc. de Hydrotech. de Fr., Paris.

Pender, D., and H. Karunarathna (2013), A statistical-process based approach for modelling beach profile variability, *Coastal Eng.*, *81*, 19–29.
Pianca, C., R. Holman, and E. Siegle (2015), Shoreline variability from days to decades: Results of long-term video imaging, *J. Geophys. Res. Oceans*, *120*, 2159–2178, doi:10.1002/2014JC010329.
Plant, N. G., R. A. Holman, M. H. Freilich, and W. A. Birkemeier (1999), A simple model for interannual sandbar behavior, *J. Geophys. Res.*, *104*(C7), 15,755–15,776.
Plant, N. G., M. H. Freilich, and R. A. Holman (2001), Role of morphologic feedback in surf zone sandbar response, *J. Geophys. Res.*, *106*(C1), 973–989.
Plant, N. G., K. T. Holland, and R. A. Holman (2006), A dynamical attractor governs beach response to storms, *Geophys. Res. Lett.*, *33*, L17607, doi:10.1029/2006GL027105.
Roelvink, D., A. Reniers, A. P. van Dongeren, J. van Thiel de Vries, R. McCall, and J. Lescinski (2009), Modelling storm impacts on beaches, dunes and barrier islands, *Coastal Eng.*, *56*(11), 1133–1152.
Roelvink, J. A., and I. Brøker (1993), Cross-shore profile models, *Coastal Eng.*, *21*(1), 163–191.
Ruessink, B. G. (2003), Intersite comparison of interannual nearshore bar behavior, *J. Geophys. Res.*, *108*(C8), 3249, doi:10.1029/2002JC001505.
Ruessink, B. G., Y. Kuriyama, A. J. H. M. Reniers, J. A. Roelvink, and D. J. R. Walstra (2007), Modeling cross-shore sandbar behavior on the timescale of weeks, *J. Geophys. Res.*, *112*, F03010, doi:10.1029/2006JF000730.
Seymour, R., R. T. Guza, W. O'Reilly, and S. Elgar (2005), Rapid erosion of a small southern California beach fill, *Coastal Eng.*, *52*(2), 151–158.
Shepard, F. P. (1950), Beach cycles in southern California, *Tech. Rep. Memo 20*, U. S. Army Corps of Eng., Washington, D. C.
Splinter, K. D., I. L. Turner, and M. A. Davidson (2013), How much data is enough? The importance of morphological sampling interval and duration for calibration of empirical shoreline models, *Coastal Eng.*, *77*, 14–27.
Splinter, K. D., I. L. Turner, M. A. Davidson, P. Barnard, B. Castelle, and J. Oltman-Shay (2014), A generalized equilibrium model for predicting daily to interannual shoreline response, *J. Geophys. Res. Earth Surf.*, *119*, 1936–1958, doi:10.1002/2014JF003106.
Stockdon, H. F., R. A. Holman, and P. A. Howd (2006), Empirical parameterization of setup, swash, and runup, *Coastal Eng.*, *53*, 573–588.
Stocker, T. F., D. Qin, G. K. Plattner, M. Tignor, S. K. Allen, J. Boschung, A. Nauels, Y. Xia, V. Bex, and P. M. Midgley (Eds.) (2013), *Climate Change 2013: The Physical Science Basis. Contribution of Working Group I to the Fifth Assessment Report of the Intergovernmental Panel on Climate Change*, Cambridge Univ. Press, Cambridge, U. K.
Stokes, C., M. Davidson, and P. Russell (2015), Observation and prediction of three-dimensional morphology at a high-energy macrotidal beach, *Geomorphology*, *243*, 1–13.
Thornton, E. B., R. T. Humiston, and W. Birkemeier (1996), Bar/trough generation on a natural beach, *J. Geophys. Res.*, *101*(C5), 12,097–12,110.
Walstra, D. J. R., A. J. H. M. Reniers, R. Ranasinghe, J. A. Roelvink, and B. G. Ruessink (2012), On bar growth and decay during interannual net offshore migration, *Coastal Eng.*, *60*, 190–200.
Wengrove, M. E., M. Henriquez, M. A. de Schipper, R. Holman, and M. J. F. Stive (2013), Monitoring morphology of the sand engine leeside using Argus cBathy, paper presented at Coastal Dynamics 2013: 7th International Conference on Coastal Dynamics, Bordeaux Univ., Arcachon, France.
Winant, C. D., D. L. Inman, and C. E. Nordstrom (1975), Description of seasonal beach changes using empirical eigenfunctions, *J. Geophys. Res.*, *80*(15), 1979–1986.
Wright, L. D., and A. D. Short (1984), Morphodynamic variability of surf zones and beaches: A synthesis, *Mar. Geol.*, *56*(1), 93–118.
Wright, L. D., A. D. Short, and M. O. Green (1985), Short-term changes in the morphodynamic states of beaches and surf zones: An empirical predictive model, *Mar. Geol.*, *62*(3–4), 339–364.
Yates, M. L., R. T. Guza, and W. C. O'Reilly (2009a), Equilibrium shoreline response: Observations and modeling, *J. Geophys. Res.*, *114*, C09014, doi:10.1029/2009JC005359.
Yates, M. L., R. T. Guza, W. C. O'Reilly, and R. J. Seymour (2009b), Overview of seasonal sand level changes on Southern California beaches, *Shore and Beach*, *77*(1), 39–46.
Yates, M. L., R. T. Guza, W. C. O'Reilly, J. E. Hansen, and P. L. Barnard (2011), Equilibrium shoreline response of a high wave energy beach, *J. Geophys. Res.*, *116*, C04014, doi:10.1029/2010JC006681.
Young, A. P., R. T. Guza, P. N. Adams, W. C. O'Reilly, and R. E. Flick (2012), Cross-shore decay of cliff top ground motions driven by local ocean swell and infragravity waves, *J. Geophys. Res.*, *117*, C06029, doi:10.1029/2012JC007908.